

PETROCHEMICAL STUDY OF THE YAMATO-691 ENSTATITE
CHONDRITE (E3) IV: DESCRIPTIONS AND MINERAL
CHEMISTRY OF OPAQUE-MINERAL NODULES

Yukio IKEDA

*Department of Earth Sciences, Faculty of Science, Ibaraki University,
1-1, Bunkyo 2-chome, Mito 310*

Abstract: Opaque-mineral nodules in Y-691 consist mainly of kamacite, perryite, schreibersite, troilite, daubreelite, niningerite, oldhamite, sphalerite, djerfisherite, caswellsilverite, graphite, roedderite, a silica mineral, albite, enstatite, and forsterite. The Ni and Si contents of kamacite are 2-3.5 wt% and about 2 wt%, respectively, being controlled by exsolution of perryite and schreibersite. Troilite shows a wide range of the Cr contents from 2.4 to 0.05 wt%, and is classified into two types, massive and porous. The massive troilite is high in the Cr contents more than 0.6 wt% and contains sometimes thin daubreelite lamellae, although the porous troilite is low in the Cr contents less than 1.2 wt% and nearly free from daubreelite lamellae. The porous texture seems to be due to tiny inclusions of FeCl₂ in the troilite. Niningerite in Y-691 is the lowest in Mn and Fe contents in comparison to those in other enstatite chondrites. Djerfisherite in Y-691 is richer in Cu, Ni and Na in comparison to those in Qingzhen. Roedderite in Y-691 is similar in chemical composition to that in Indarch. Enstatite in Y-691 nodules shows a wide range of MgO/(MgO+FeO) molar ratio from 0.91 to 0.99, and sometimes forsterite occurs with a silica mineral in a nodule, suggesting that the silicates in the opaque-mineral nodules were not in equilibrium.

Opaque-mineral nodules were classified into two main types based on the texture; concentric and massive, which are further divided into subtypes based on the modal volume of the main-minerals. The constituent minerals in these nodules seem to have polygenesis, and the genesis of nodules is discussed in detail. Any thermal metamorphic effects after accretion was not petrographically detected in Y-691 nodules.

1. Introduction

The Y-691 enstatite chondrite has been studied as a consortium study for three years from 1984 to 1987, and this paper is one of the consortium studies, concentrating on descriptions and mineral chemistry of opaque-mineral nodules. The preceding papers (IKEDA, 1988a, b, 1989) deal with bulk compositions, descriptions and mineral chemistry of unusual silicate-inclusions and chondrules in Y-691.

Opaque minerals in enstatite chondrites are considered to have been formed under an extremely-reduced condition in the protosolar nebula and in the parent body. Most enstatite chondrites had more or less suffered from thermal metamorphism in the parent body (LARIMER *et al.*, 1974; WEAKS *et al.*, 1985), and the opaque minerals in those enstatite chondrites had been changed from the original occurrence and mineral chemistry by the thermal metamorphism. However, the Y-691 chondrite has

not suffered from remarkable metamorphism in the parent body, because clean glasses occur in some chondrules, outlines of chondrules are very sharp, and the MgO/(MgO+FeO) ratios of silicates range widely from 0.74 to 1.00 (IKEDA, 1988b, 1989). Therefore, opaque minerals in Y-691 may remain as they were produced in the protosolar nebula in an extremely-reduced condition.

The mineral compositions of opaque minerals in Y-691 were reported by OKADA (1975) and PRINZ *et al.* (1984). EL GORESY *et al.* (1988) studied the mineral chemistry and the genesis of opaque-mineral nodules as one of the Y-691 consortium studies. The purposes of this paper are to describe opaque minerals and the associating silicates in Y-691 and to clarify their origin and genetical relationships.

2. Analytical Method

Opaque minerals and silicates were analysed using an electron-probe micro-analyser (EPMA, JEOL-Superprobe 733, sample-current of 3–5 nA, accelerating voltage of 15 kV). Correction method of standard ZAF for opaque minerals was applied, and the method of BENCE and ALBEE (1967) was used for silicates.

3. General Description

The Y-691 enstatite chondrite consists of unusual silicate-inclusions, chondrules, opaque-mineral nodules, mineral fragments, and matrix (IKEDA, 1988a, b, 1989). Opaque minerals in Y-691 occur mainly as nodules and small fragments, and minor amounts are in unusual silicate-inclusions and chondrules. Opaque-mineral nodules are similar in size to chondrules and are aggregates consisting mainly of opaque minerals such as metal, sulfide, phosphide and silicide with or without small amounts of silicates. They are classified into two main types, concentric nodules and massive nodules, which are further divided into subtypes, as follows.

- * Concentric nodules {
 - Kamacite-core nodules
 - Sulfide-core nodules

- * Massive nodules {
 - Kamacite nodules
 - Kamacite-troilite nodules
 - Kamacite-niningerite nodules
 - Troilite nodules
 - Niningerite-troilite nodules
 - Djerfisherite-troilite nodules

The concentric nodules show a concentric structure consisting of a kamacite-sulfide core and a kamacite-sulfide mantle with or without middle zone between core and mantle. They are subdivided into two types based on the predominant phase in the core. On the other hand, the other main type, massive nodules, does not show such a concentric structure. Kamacite (Ka) nodules and troilite (Tr) nodules are subtypes of massive nodules in which kamacite and troilite are predominant (more than 90 volume %), respectively. Ka-Tr or Ka-niningerite (Nin) nodules include both kamacite

and troilite or kamacite and niningerite as main phases, respectively. Nin-Tr or djerfisherite (Djer)-Tr nodules consist mainly of niningerite and troilite or djerfisherite and troilite, respectively. In Y-691, Ka-Tr nodules are the most abundant, Ka-core, sulfide-core, and Ka nodules are common, and Ka-Nin, Tr, Nin-Tr, or Djer-Tr nodules are rare. Intermediate types between the main types and among the subtypes are observed.

4. Description of Opaque-mineral Nodules

4.1. Kamacite-core nodules

Nodule No. 502-I shows a concentric structure consisting of a kamacite and troilite core, silicate middle zone, and a kamacite and troilite mantle (Fig. 1a, left). The core includes small oldhamite (Fig. 1b). The middle zone is partly lacking, where troilite occurs continuously from core to mantle, and it consists mainly of a silica mineral and niningerite (Fig. 1b) with minor amounts of enstatite and troilite. The mantle is kamacite and troilite with a small amount of perryite. The perryite is included by troilite in the mantle.

Nodule No. 507 shows a weak concentric structure with kamacite-predominant core and mantle (Fig. 2a). Between the core and mantle, a silica mineral, forsterite with $Mg/(Mg+Fe)$ ratio (hereafter, *mg* value) of 0.99, and enstatite with *mg* value of 0.97 occur irregularly, and the forsterite is always surrounded by enstatite (Fig. 2b). Small amounts of perryite and troilite occur in the mantle, and schreibersite is observed in the core.

Nodule No. 511 shows a concentric structure, consisting of a kamacite core, kamacite and silicate middle zone, and a kamacite mantle (Fig. 3). The silicate in the middle zone is almost a silica mineral, and perryite occurs in a small amount between the core and the middle zone. Minor troilite occurs in the mantle and the middle zone.

Nodule No. 512 consists of a kamacite core, silicate and sulfide middle zone, and a kamacite mantle (Fig. 4a). The core is mainly kamacite with small grains of schreibersite, and troilite occurs as a vein protruding the core. The middle zone consists of troilite, niningerite, and enstatite ($mg=0.99$) with small amounts of albite and a silica mineral, where enstatite is surrounded by niningerite (Fig. 4b). The mantle is mainly kamacite with a small amount of troilite.

Nodule No. 516-I shows a weak concentric structure, the core and mantle being mainly kamacite including small perryite grains (Fig. 5a). Between the core and mantle, silicates and troilite occur irregularly, and the silicates are a silica mineral, forsterite ($mg=0.97$), and enstatite ($mg=0.97$) (Fig. 5b).

The core and mantle in nodule No. 517 consist of kamacite with small amounts of perryite, niningerite, and troilite (Fig. 6a). The middle zone consisting of a silica mineral, troilite, and minor sphalerite is weakly recognized (Fig. 6b).

In nodule No. 538, the core consists of kamacite with small amounts of troilite, niningerite, and albite (Fig. 7). Albite ($Ab_{99.6}Or_{0.4}$) occurs as a small grain between niningerite and kamacite. The mantle consists mainly of kamacite with small amounts of troilite and a Cr-bearing phase (which may be altered caswellsilverite).

In nodule No. 539, the core consists of kamacite with small amounts of troilite and niningerite (Fig. 8). The mantle consists of kamacite with small amounts of troilite and perryite. The middle zone consisting mainly of enstatite ($mg=0.97$) and troilite is weakly recognized.

4.2. Sulfide core nodules

Nodule 502-II consists of a niningerite and roedderite core and a kamacite mantle (Fig. 1a, right). The roedderite shows a euhedral form in niningerite.

Nodule No. 528 consists of a troilite and niningerite core and a kamacite and troilite mantle (Fig. 9a). A large troilite grain occurs in the central portion of the core, surrounded by niningerite. The niningerite includes small needle crystals of troilite, which arrange in the three different orientations (Fig. 9b). The mantle consists of an aggregate of kamacite and troilite with small amounts of perryite, schreibersite, and enstatite (Fig. 9c).

In nodule No. 548, the core is mainly niningerite with small amounts of troilite, a Na-Cr-S phase and perryite (Fig. 10). The mantle consists mainly of kamacite.

4.3. Kamacite nodules

Nodule No. 500 (Fig. 11a) consists of kamacite with small amounts of troilite, schreibersite, oldhamite, sphalerite, graphite and perryite. The nodule includes a small hexagon-shaped inclusion in the central portion which consists of troilite with daubreelite lamellae, schreibersite, oldhamite, perryite, and sphalerite (Fig. 11b). Oldhamite and sphalerite occur in the central portion of the hexagon-shaped inclusion, surrounded by troilite. The hexagon-shaped inclusion is partially surrounded by irregular perryite. Besides the hexagon-shaped inclusion, the nodule includes a graphite inclusion and several irregular patches of troilite and schreibersite.

Nodule No. 513-I (Fig. 12a) consists of kamacite with small amounts of troilite, oldhamite, niningerite, perryite and silicates. The silicates are enstatite ($mg=0.97$) and albite (Fig. 12b). A small albite grain occurs in contact with oldhamite (Fig. 12b), and the composition is $An_1Ab_{98}Or_1$.

Nodule No. 537 (Fig. 13a) consists of kamacite and minor troilite with small amounts of perryite, niningerite, albite, enstatite ($mg=0.98$) and a silica mineral. Albite occurs in contact with troilite (Fig. 13b), and the composition is $Ab_{99.7}Or_{0.3}$.

4.4. Kamacite-troilite nodules

Nodule No. 503 (Fig. 14a) consists of troilite and kamacite with small amounts of schreibersite, perryite, djerfisherite and a Cr-bearing phase. Troilite is a major phase in the nodule, showing two kinds of appearance under the microscope or in back-scattered-electron (BSE) image: massive troilite and porous troilite (Fig. 14b). The porous troilite includes many tiny pits of about one micron in size, whereas the massive one does not. Djerfisherite occurs as small grains included by the porous troilite (Fig. 14b). A large kamacite occurs in the central portion of the nodule showing an irregular outline. Schreibersite occurs as small rounded inclusions in kamacite and troilite, and the schreibersite between kamacite and troilite protrudes the surrounding troilite (Fig. 14c). A Cr-bearing phase (Fig. 14a) occurs in troilite, which

may have been originally caswellsilverite.

Nodule No. 501 (Fig. 15a) consists of troilite, kamacite, and niningerite with small amounts of perryite, oldhamite and silicates. Kamacite occurs as irregular grains. Many rounded tiny grains of schreibersite are observed in troilite, and porous troilite occurs between kamacite and massive troilite (Fig. 15b). A small grain of a Cr-bearing phase occur between kamacite and niningerite (Fig. 15c). A silicate aggregate occurs in the central portion of the nodule (Fig. 15a), and it consists of a silica mineral, enstatite, forsterite, and troilite (Fig. 15d).

Nodule No. 508-I (Fig. 16a) consists of kamacite and troilite with small amounts of perryite, schreibersite and caswellsilverite. Caswellsilverite occurs in the central portion of the nodule and is partly altered to Na-depleted Cr-bearing phases (Fig. 16b).

Nodule No. 509 (Fig. 17a) consists of troilite with small amounts of kamacite, niningerite, and schreibersite. The troilite shows two appearance; massive and porous (Fig. 17b). The massive troilite includes thin daubreelite lamellae whereas the latter does not. Schreibersite occurs as small rounded grains in kamacite and troilite (Fig. 17b).

Nodule No. 529 (Fig. 18) is an aggregate of kamacite, minor troilite, silicates, and perryite. The silicates are a silica mineral and enstatite ($mg=0.98$).

4.5. Kamacite-niningerite nodules

In nodule No. 516-II, kamacite and niningerite are main phases, and troilite, sphalerite, schreibersite, perryite, and a Cr-bearing phase occur in small amounts (Fig. 19a). The sphalerite occurs as a relatively large grain including several rounded tiny schreibersite grains (Fig. 19b).

4.6. Troilite nodules

Nodule No. 506 is a troilite nodule (Fig. 20a), consisting of porous troilite with small amounts of kamacite, sphalerite and schreibersite. Sphalerite occurs as small grains in troilite and shows a porous texture similar to the porous troilite (Fig. 20b).

Nodule No. 601 (Fig. 21a) consists mainly of porous troilite, including small amounts of sphalerite, enstatite, and a silica mineral. The sphalerite shows a porous texture similar to that in No. 506 (Fig. 21b). Enstatite occurs as rectangular laths (Fig. 21b).

Nodule No. 602 (Fig. 22) consists of massive troilite, showing a spherical outline. Albite is included in troilite, and the composition is $Ab_{99.5}Or_{0.5}$.

Nodule No. 531 (Fig. 23a) consists of troilite and silicates. Troilite is massive one including daubreelite lamellae. Silicates are enstatite, roedderite, and a silica mineral. Enstatite shows a euhedral form included in troilite (Fig. 23a), and the mg value is about 0.99. A small grain of roedderite occurs in association with a silica mineral (Fig. 23b), and some silica-mineral blebs are included in troilite (Fig. 23b).

Nodule No. 532 (Fig. 24) consists mainly of troilite, including silicates in small amounts. Silicates are roedderite and a silica mineral, and the roedderite shows a rectangular euhedral form in the nodule (Fig. 24).

4.7. *Ninningerite-troilite nodules*

Nodule No. 530 (Fig. 25) consists mainly of niningerite and troilite. Troilite is massive one including daubreelite lamellae. A euhedral crystal of roedderite is included completely by niningerite.

4.8. *Djerfisherite-troilite nodules*

Nodule No. 504 is a djerfisherite-troilite nodule (Fig. 26a), consisting of djerfisherite and porous troilite with small amounts of niningerite, oldhamite, kamacite, a Cu-bearing phase, and silicates. Djerfisherite is a major phase in the nodule. Troilite occurs as lamellae in djerfisherite and as rims surrounding djerfisherite grains. The troilite lamellae in the host djerfisherite show two different orientations (Fig. 26b). Ninningerite occurs as large rounded or rectangular grains. Rare kamacite is included in troilite. Oldhamite occurs as small irregular grains in the nodule (Fig. 26c). A Cu-bearing phase occurs in djerfisherite and/or troilite and shows a unique striped pattern (Fig. 26d). The silicates are forsterite, enstatite and a silica mineral. Forsterite is surrounded by or includes tiny troilite grains (Fig. 26e). Enstatites are CaO-rich and CaO-poor ones. The former occurs with olivine (Fig. 26e) and the CaO content is about 2 wt%, and the latter occurs as large rounded grains (Fig. 26f) and the CaO content is less than 0.5 wt%. The *mg* values are about 0.99 for forsterite and 0.91–0.99 for CaO-poor enstatite, and the chemical composition of CaO-rich enstatite is $\text{En}_{92-94}\text{Fs}_{2-4}\text{Wo}_4$.

Nodule No. 543 consists of djerfisherite and porous troilite with small amounts of silicates (Fig. 27a). Djerfisherite grains are always surrounded by porous troilite. Silicates are mainly enstatite (*mg*=0.98) and minor albite, and a small grain of albite is completely surrounded by enstatite (Fig. 27b).

5. Mineralogy

5.1. *Kamacite, (Fe, Ni)*

Kamacite occurs commonly in nodules of Y-691, but taenite does not occur. The chemical compositions are shown in Table 1. As shown in Figs. 28(a) and 29(a), Ni, Si, and Co contents of kamacite are 2.0–3.7, 1.7–2.3, and 0.2–0.4 wt%, respectively. In Figs. 28(b) and 29(b), kamacites from EH chondrites, EL chondrites and aubrites are plotted for comparison. Kamacites in EH chondrites seem to separate into two groups, which was already shown by RAMBALDI *et al.* (1983); low-Ni (Ni=2–4 wt%) and high-Ni (Ni=6–7 wt%) groups. The chemical compositions of kamacite in Y-691 coincide with those of low-Ni group of EH chondrites.

The Ni content of kamacite in Y-691 nodules varies among nodules or in a nodule. Generally speaking, kamacite grains which seem to be relic after the sulfurization to produce troilite show systematic difference in Ni content; the peripheral portion of the kamacite is higher in Ni content than the central portion, suggesting that Ni content of peripheral kamacite was piled up at the front of troilite formation during sulfurization. Therefore, one explanation for the wide range in Ni content is replacement of kamacite by troilite.

On the assumption that Y-691 kamacite containing about 2 wt% Si was in equi-

Table 1. The chemical compositions of kamacites in Y-691. The numbers at the top of each column are nodule-numbers, and the abbreviations, Ka-core, S-core, Ka, Ka-Tr, Ka-Ni, Tr, and Dj-Tr are kamacite-core, sulfide-core, kamacite, kamacite-troilite, kamacite-niningerite, troilite, and djerfisherite-troilite subtypes of nodules, respectively.

	1	2	3	4	5	6	7	8	9	10	11	12	13	14	15	16	17
2		500	500	500	501	501	502-I	502-I	502-II	503	503	504	505	505	505	506	507
3		Ka			Ka-Tr		Ka-core		S-core	Ka-Tr		Dj-Tr	Ka			Tr	Ka-core
4 Si		2.19	2.11	2.15	2.21	1.92	1.96	1.80	2.04	1.89	1.88	1.85	1.99	2.10	2.10	1.89	2.29
5 P		0.00	0.00	0.00	0.02	0.00	0.00	0.00	0.00	0.00	0.00	0.03	0.02	0.00	0.00	0.01	0.03
6 Cr		0.01	0.02	0.00	0.00	0.01	0.00	0.00	0.01	0.00	0.01	0.02	0.01	0.00	0.00	0.00	0.02
7 Fe		94.35	93.40	94.06	94.01	95.55	94.37	95.64	95.69	94.87	94.40	94.74	95.08	94.65	95.34	93.91	94.51
8 Co		0.30	0.24	0.32	0.30	0.36	0.20	0.22	0.31	0.38	0.37	0.33	0.27	0.29	0.22	0.23	0.21
9 Ni		3.35	3.36	3.49	3.25	2.64	3.30	2.29	2.00	3.19	3.04	3.44	3.08	3.44	2.52	3.23	2.44
10 Total		100.20	99.13	100.02	99.79	100.48	99.83	99.95	100.05	100.33	99.70	100.41	100.45	100.48	100.18	99.27	99.50

	18	19	20	21	22	23	24	25	26	27	28	29	30	31	32	33	34
2		507	507	508-I	508-I	509	509	510	510	511	511	511	511	512	512	512	513-I
3				Ka-Tr		Ka-Tr		Ka-core		Ka-core				Ka-core			Ka
4 Si		1.88	1.85	2.15	2.09	1.99	1.95	2.05	1.99	2.10	2.12	2.26	1.99	1.91	1.90	2.07	1.98
5 P		0.00	0.03	0.01	0.00	0.05	0.01	0.00	0.04	0.00	0.00	0.00	0.02	0.00	0.00	0.00	0.00
6 Cr		0.02	0.00	0.01	0.01	0.00	0.05	0.02	0.00	0.00	0.00	0.00	0.05	0.02	0.00	0.00	0.00
7 Fe		94.79	95.80	94.75	94.79	93.83	94.83	95.13	94.25	95.82	94.12	95.13	94.37	94.54	95.43	94.71	95.38
8 Co		0.36	0.32	0.30	0.24	0.41	0.28	0.27	0.35	0.36	0.29	0.30	0.28	0.38	0.20	0.29	0.30
9 Ni		2.74	2.21	2.71	2.52	3.25	2.97	3.40	3.39	2.47	3.00	2.36	2.78	2.44	2.38	2.82	2.19
10 Total		99.79	100.21	99.93	99.65	99.53	100.09	100.87	100.02	100.75	99.53	100.05	99.49	99.29	99.91	99.89	99.85

	35	36	37	38	39	40	41	42	43	44	45	46	47	48	49	50	51
2		513-I	513-I	516-I	516-II	517	528	528	528	529	537	538	538	539	539	548	548
3				Ka-core	Ka-Ni	Ka-core	S-core			Ka-Tr	Ka	Ka-core		Ka-core		S-core	
4 Si		2.02	1.71	1.92	2.16	2.06	2.13	1.74	1.63	2.05	1.92	1.72	1.86	2.11	1.78	2.09	1.96
5 P		0.00	0.01	0.00	0.00	0.02	0.00	0.00	0.00	0.02	0.04	0.00	0.02	0.01	0.07	0.00	0.03
6 Cr		0.00	0.05	0.02	0.00	0.02	0.00	0.00	0.07	0.07	0.05	0.02	0.01	0.00	0.02	0.07	0.00
7 Fe		94.34	95.34	94.54	94.32	95.49	95.72	95.45	95.80	92.92	94.49	96.70	94.19	94.03	95.51	95.84	94.43
8 Co		0.26	0.34	0.31	0.23					0.38			0.35	0.40	0.30		0.32
9 Ni		3.27	2.46	3.09	2.51	2.60	2.42	2.54	2.67	3.06	3.17	2.36	2.92	3.72	2.80	2.77	3.28
10 Total		99.89	99.91	99.88	99.22	100.19	100.27	99.73	100.17	98.50	99.67	100.80	99.35	100.27	100.48	100.77	100.02

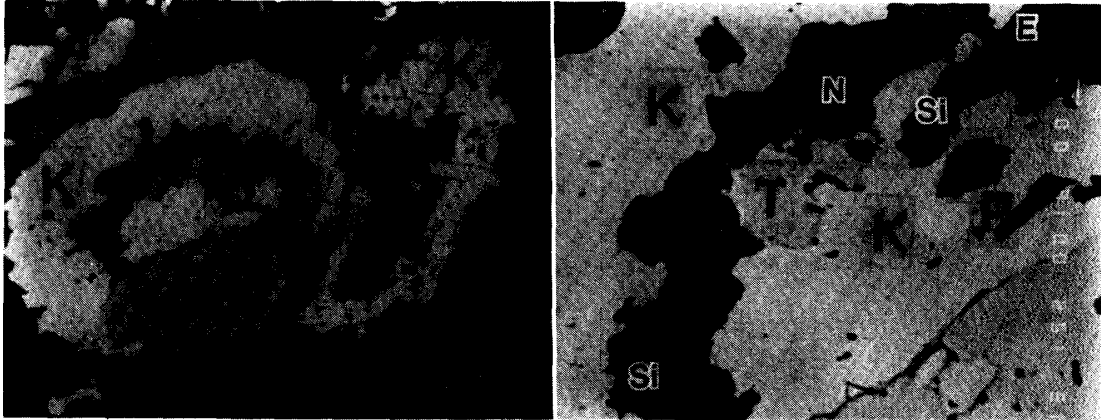


Fig. 1a. Photomicrograph (reflected light) of No. 502-I (left) and No. 502-II (right). K, T, P, O, N, and R are kamacite, troilite, perryite, oldhamite, niningerite, and roedderite, respectively. The same abbreviations are used in the following figures. Width of figure is 300 μm .

Fig. 1b. Back-scattered-electron (BSE) image of the upper-left portion of No. 502-I (Fig. 1a). The abbreviation Si is a silica mineral. The middle zone consists mainly of niningerite and a silica mineral. Width is 73 μm .

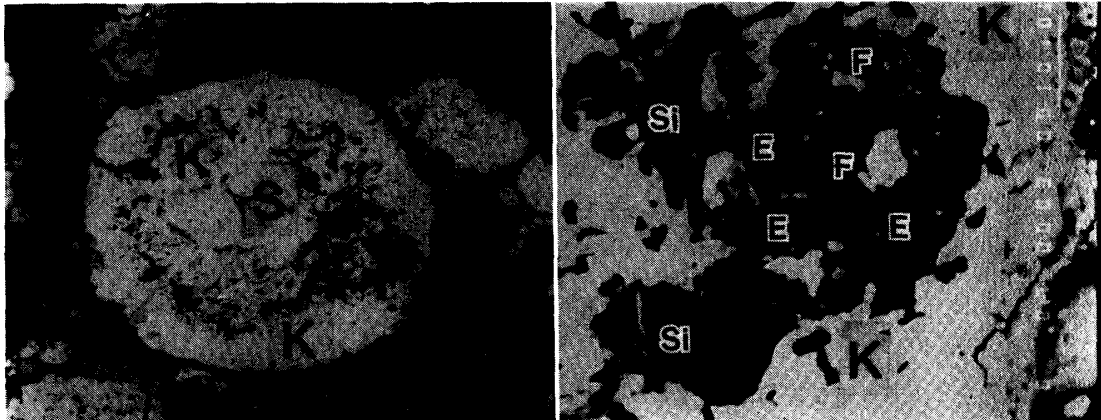


Fig. 2a. Photomicrograph (ref. light) of No. 507. The abbreviation S is schreibersite. Width is 600 μm .

Fig. 2b. BSE image of the right portion of No. 507. The abbreviations, E and F, are enstatite and forsterite, respectively. Forsterite is surrounded by enstatite. Width is 60 μm .

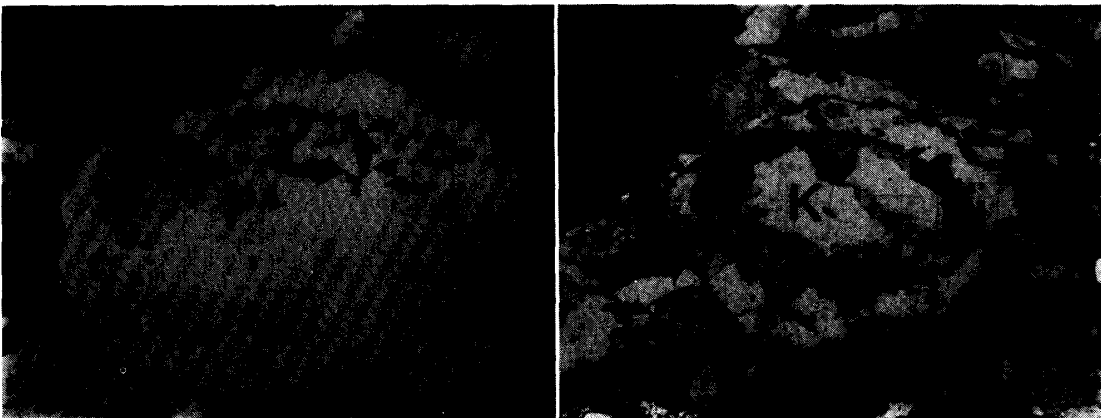


Fig. 3. Photomicrograph (ref. light) of No. 511. Black portions in the middle zone are mainly a silica mineral. Width is 300 μm .

Fig. 4a. Photomicrograph (ref. light) of No. 512. Width is 600 μm .

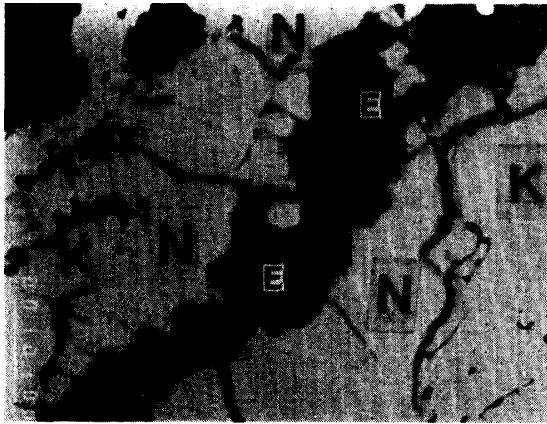


Fig. 4b. BSE image of the upper-left portion of No. 512, where enstatite is embedded by niningerite. Width is 56 μm .

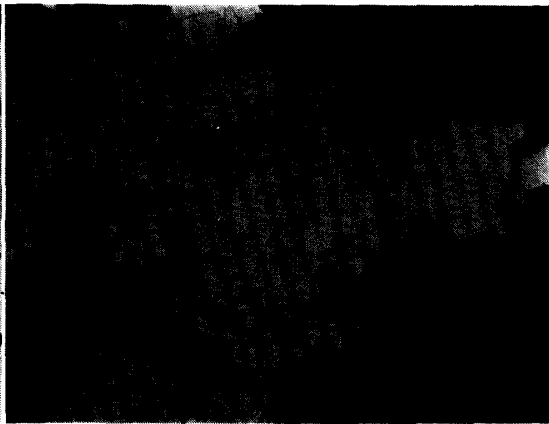


Fig. 5a. Photomicrograph (ref. light) of No. 516-I. Width is 300 μm .

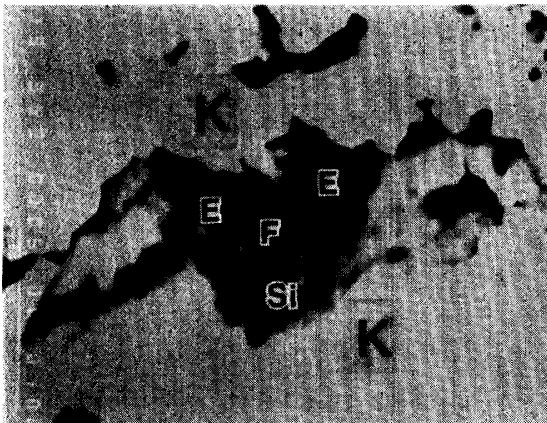


Fig. 5b. BSE image of the upper portion of No. 516-I, where forsterite coexists with enstatite and a silica mineral. Width is 30 μm .

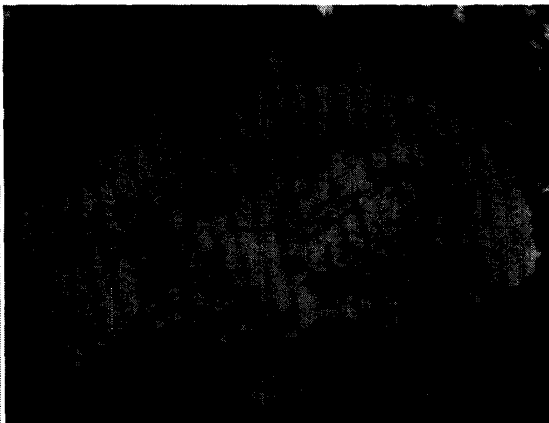


Fig. 6a. Photomicrograph (ref. light) of No. 517. Width is 600 μm .

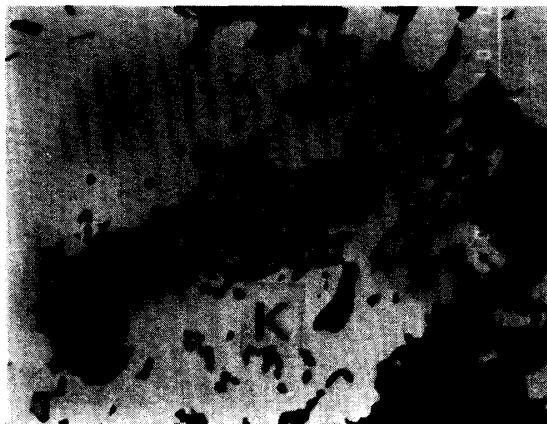


Fig. 6b. BSE image of the upper-right portion of No. 517. The abbreviation Sp is sphalerite, and black portions of figure are mainly a silica mineral. Width is 56 μm .



Fig. 7. Photomicrograph (ref. light) of No. 538. An albite grain (A, black in figure) occurs in contact with niningerite. Width is 300 μm .

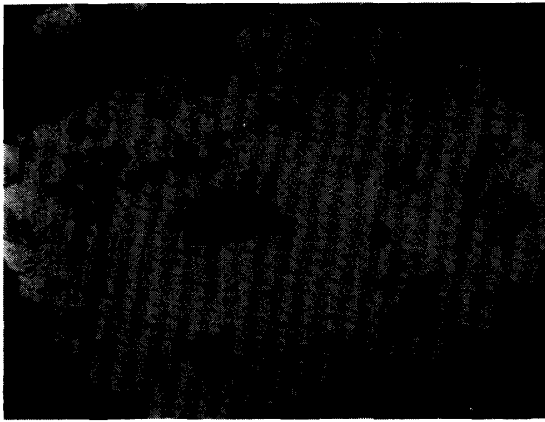


Fig. 8. Photomicrograph (ref. light) of No. 539. Black portions in the middle zone are mainly enstatite. Width is 300 μm .

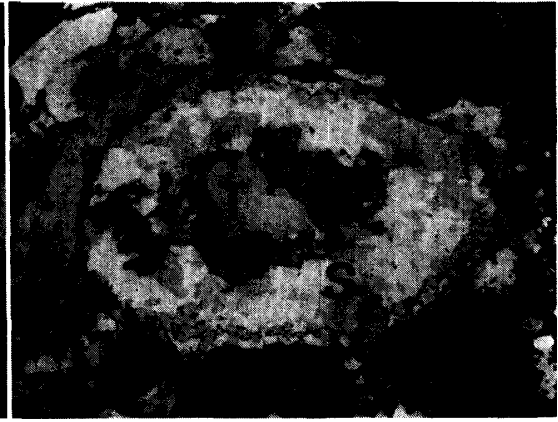


Fig. 9a. Photomicrograph (ref. light) of No. 528. Width is 600 μm .

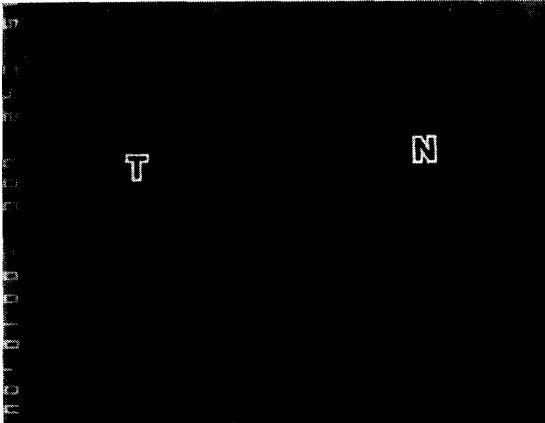


Fig. 9b. BSE image of the central portion of No. 528. Note that small needle crystals of troilite show three different orientations in the niningerite host. Width is 45 μm .

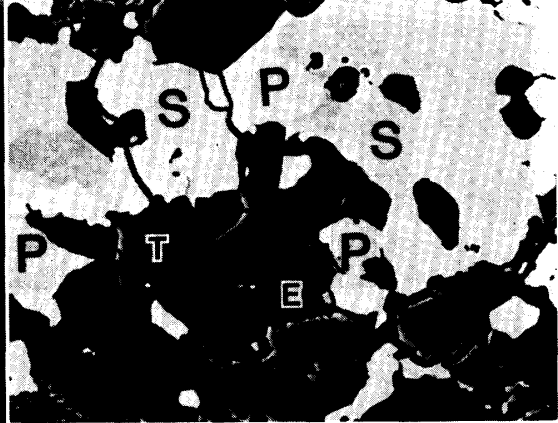


Fig. 9c. BSE image of the lower-right portion of No. 528. Irregularly-shaped perryite and rounded schreibersite grains occur in kamacite. Enstatite is surrounded mostly by troilite and partly by perryite. Width is 86 μm .



Fig. 10. Photomicrograph (ref. light) of No. 548. The abbreviation Cr is a Na-Cr-S phase. Width is 300 μm .

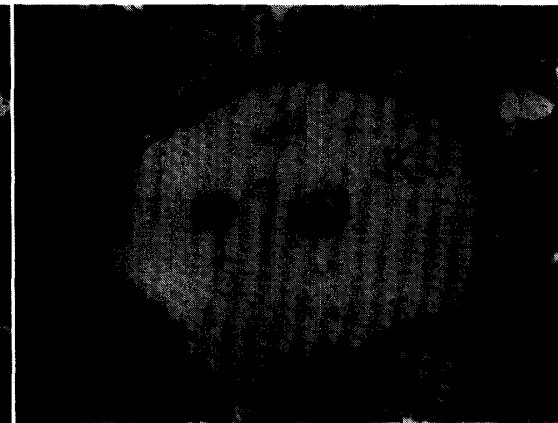


Fig. 11a. Photomicrograph (ref. light) of No. 500. Width is 1200 μm .

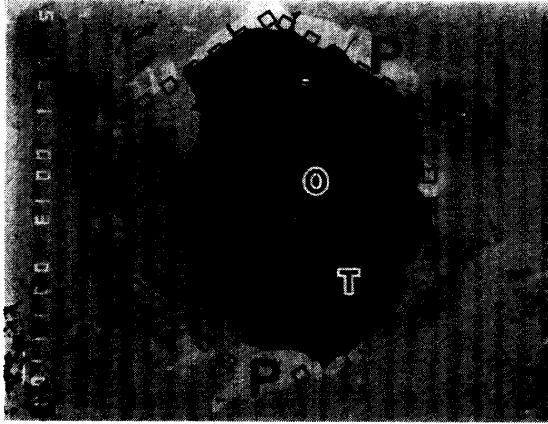


Fig. 11b. BSE image of the central portion of No. 500. Note the hexagon-shaped inclusion (shown by open squares) surrounded by kamacite and partly by perryite. Width is 170 μm .

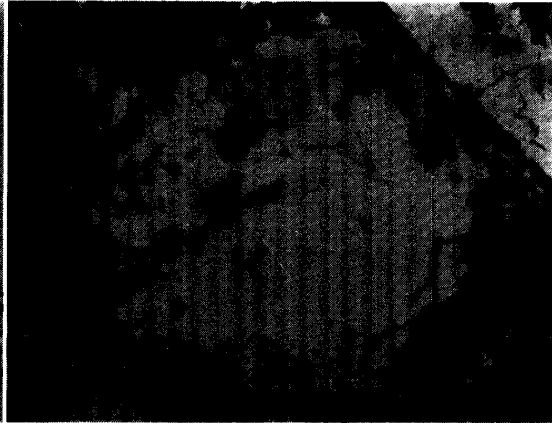


Fig. 12a. Photomicrograph (ref. light) of No. 513-I. Width is 300 μm .

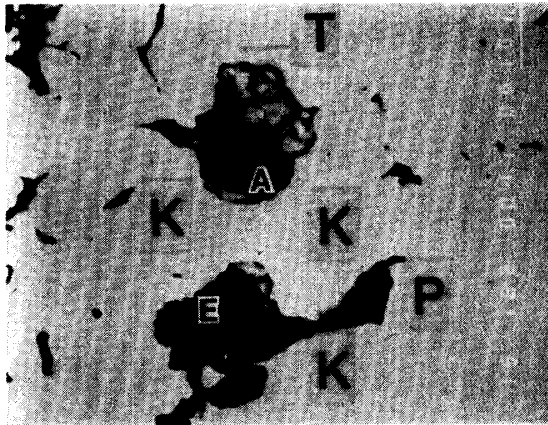


Fig. 12b. BSE image of the upper portion of No. 513-I, where a small oldhamite grain occurs between a large troilite and a small albite. Width is 68 μm .

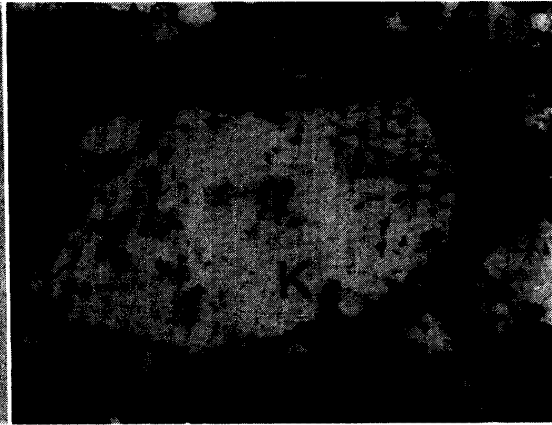


Fig. 13a. Photomicrograph (ref. light) of No. 537. Black portions in figure are mainly silicates. Width is 600 μm .

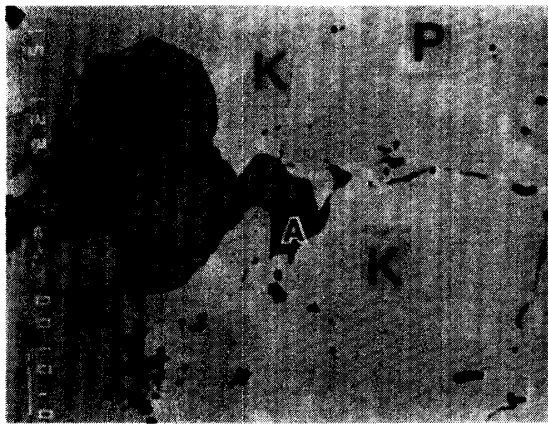


Fig. 13b. BSE image of the central portion of No. 537, where a small albite grain (A) occurs between kamacite and troilite. Small perryite grains are observed in kamacite. Width is 86 μm .

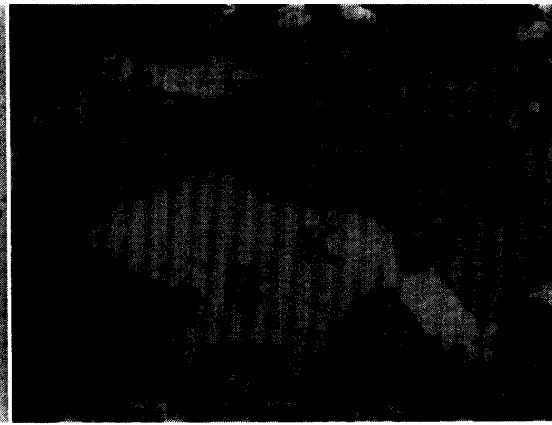


Fig. 14a. Photomicrograph (ref. light) of No. 503. Small rounded schreibersite grain occur in troilite and kamacite. A large grain of a Na-Cr-S phase (Cr) is observed in the upper-central portion. Width is 600 μm .



Fig. 14b. BSE image of the right portion of No. 503. The abbreviations, D, pT, and mT are djerfisherite, porous troilite, and massive troilite, respectively. Small djerfisherite grains are completely surrounded by porous troilite. Width is 250 μm .



Fig. 14c. BSE image of the lower portion of No. 503. Rounded grains of schreibersite occur in porous troilite, and a rounded schreibersite grain (the central portion of figure) protrudes into porous troilite. Similar rounded schreibersite grains occur in kamacite (Fig. 14a). Width is 140 μm .

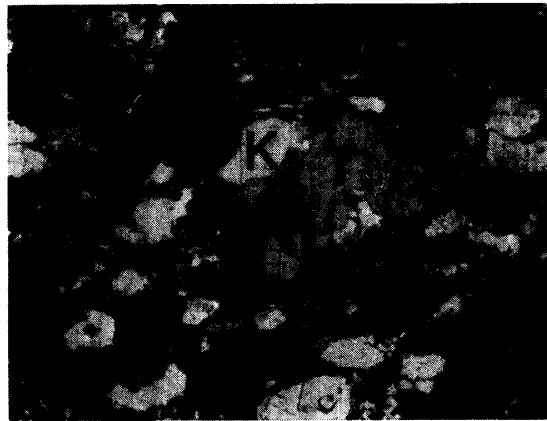


Fig. 15a. Photomicrograph (ref. light) of No. 501. A silicate aggregate (SL) occurs in the central portion of figure. Width is 1200 μm .



Fig. 15b. BSE image of the upper-right portion of No. 501. Small rounded grains of schreibersite occur in massive troilite. Porous troilite is observed between kamacite and massive troilite. Width is 136 μm .

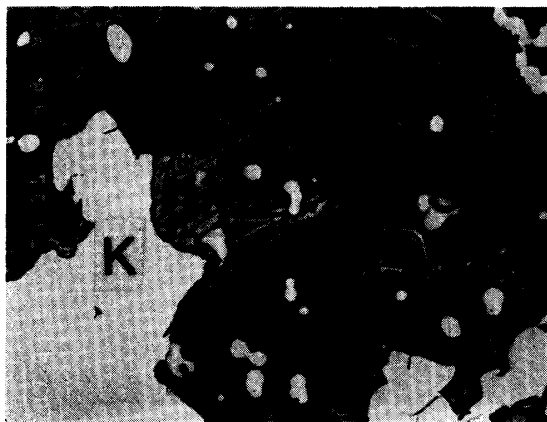


Fig. 15c. BSE image of the left portion of No. 501. A Na-Cr-S grain (Cr) occurs between kamacite and niningerite. Small rounded grains of schreibersite similar to those in Fig. 15b are observed in niningerite. Width is 136 μm .

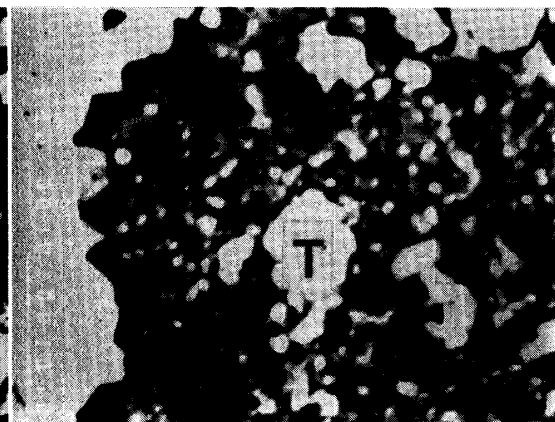


Fig. 15d. BSE image of the central portion of No. 501. A silicate aggregate (SL in Fig. 15a) consists of forsterite, enstatite, and a silica mineral with small troilite grains. Width is 35 μm .



Fig. 16a. Photomicrograph (ref. light) of No. 508-I. An aggregate of Na-Cr-S phase (Cr) occurs in the central portion. Width is 600 μm .



Fig. 16b. BSE image of a Na-Cr-S aggregate (Cr) in No. 508-I. A fresh caswellsilverite (NaCrS_2) is detected in the central portion. Width is 110 μm .

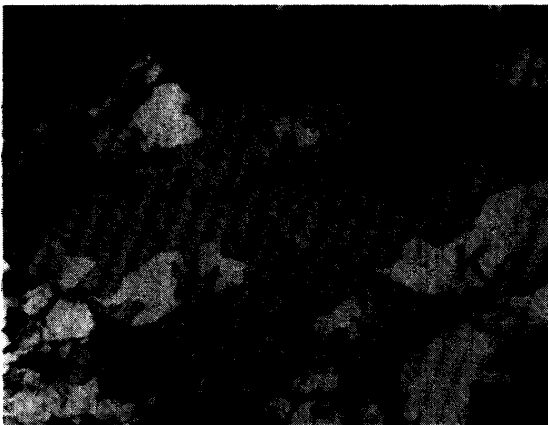


Fig. 17a. Photomicrograph (ref. light) of No. 509. Width is 600 μm .



Fig. 17b. BSE image of the central portion of No. 509. Massive and porous troilite are observed. Small schreibersite grains occur in massive and porous troilite.



Fig. 18. Photomicrograph (ref. light) of No. 529. Black portions in figure are mainly silicates. Width is 300 μm .

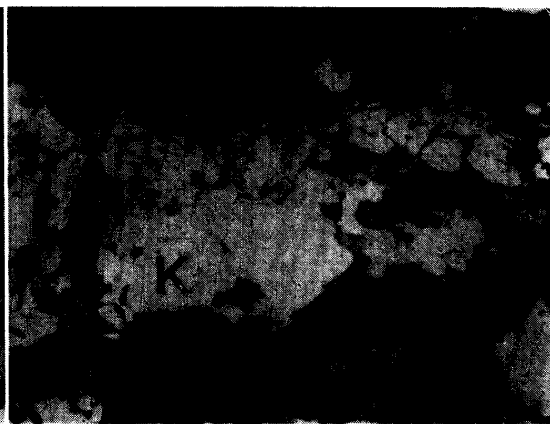


Fig. 19a. Photomicrograph (ref. light) of No. 516-II. A large sphalerite grain occurs in the right portion of figure. Width is 300 μm .



Fig. 19b. BSE image of sphalerite in No. 516-II. Small rounded schreibersite grains occur in sphalerite and kamacite. Sphalerite seems to have been formed by replacement of kamacite. A Na-Cr-S grain (Cr) is observed in the upper portion. Width is 63 μm .

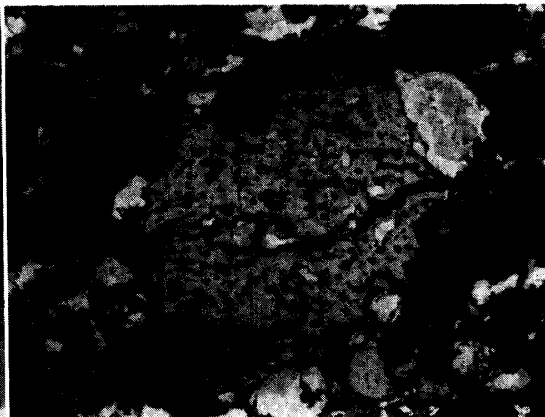


Fig. 20a. Photomicrograph (ref. light) of No. 506. Width is 600 μm .

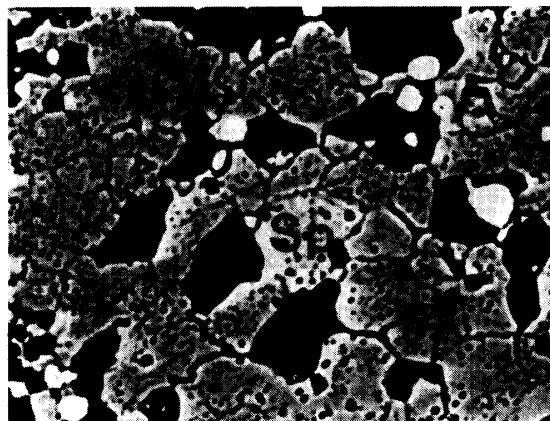


Fig. 20b. BSE image of the upper-left portion of No. 506. Sphalerite is observed in the central portion, showing a porous texture similar to that of porous troilite. Width is 63 μm .

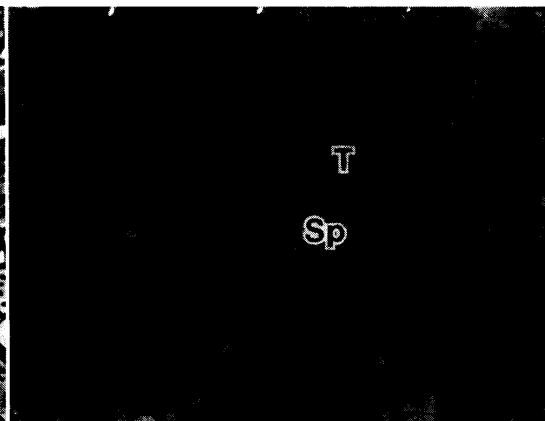


Fig. 21a. Photomicrograph (ref. light) of No. 601. Width is 480 μm .

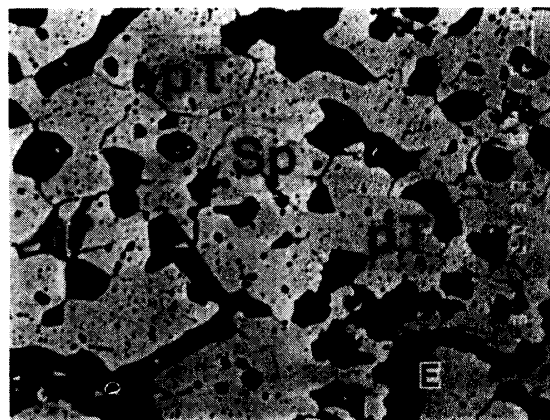


Fig. 21b. BSE image of the central portion of No. 601. Sphalerite is observed in the central portion, and elongated laths of enstatite (E) occur in porous troilite. Width is 86 μm .

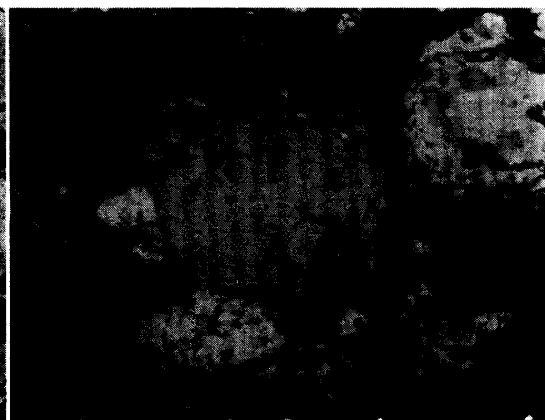


Fig. 22. Photomicrograph (ref. light) of No. 602. Small albite grains (A) occur in massive troilite. Width is 480 μm .



Fig. 23a. BSE image of No. 531. Large and small euhedral enstatite and a silicate aggregate (SL) are observed in massive troilite. Width is 280 μm .

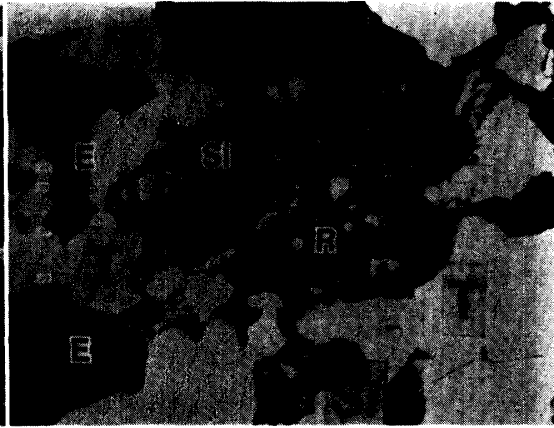


Fig. 23b. BSE image of a silicate aggregate in No. 531. A small roedderite grain coexists with a silica mineral and minor troilite. Width is 95 μm .

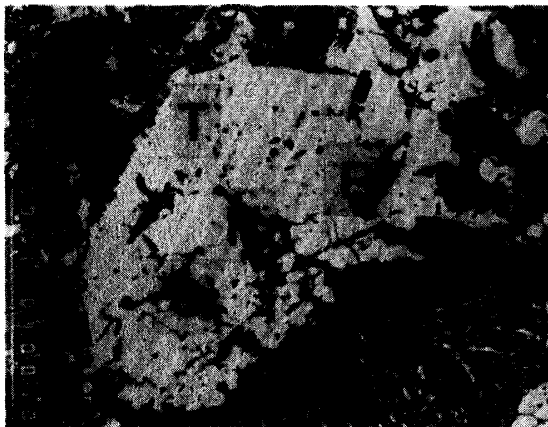


Fig. 24. BSE image of No. 532. Elongated laths of roedderite and a silica mineral occur in troilite. Width is 230 μm .

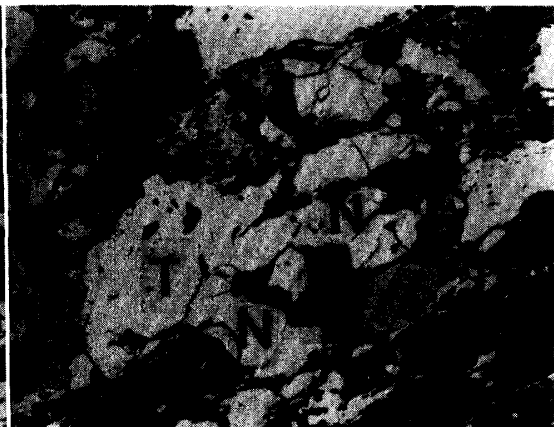


Fig. 25. BSE image of No. 530. A large rectangular lath of roedderite is included by ningerite. Width is 280 μm .

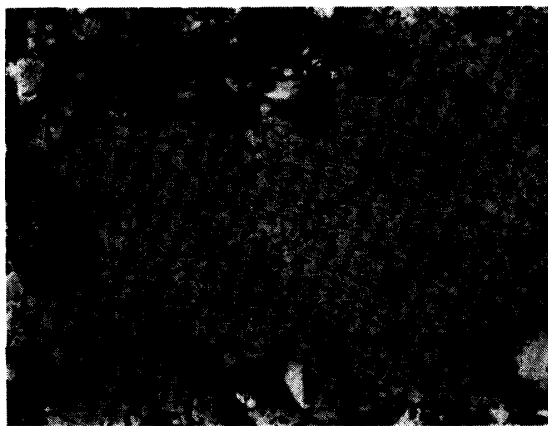


Fig. 26a. Photomicrograph (ref. light) of No. 504. A large rounded ningerite (N) occurs in the left portion of figure. A rounded silicate aggregate (SL) is observed in the lower-left portion. Width is 1200 μm .

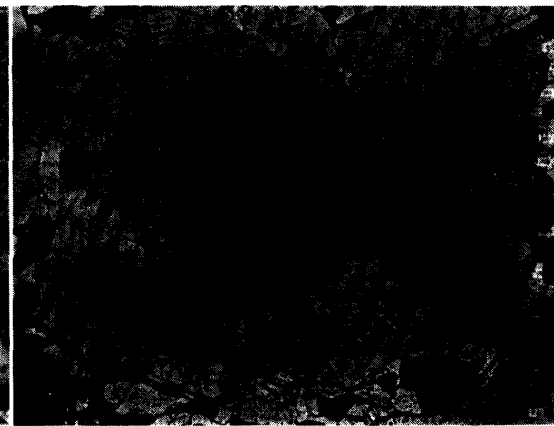


Fig. 26b. BSE image of the upper-right portion of No. 504. Note the two different orientations of porous troilite lamellae in a large djerfisherite crystal. A Cu-S-O phase (Cu) is observed in the lower portion. Width is 170 μm .



Fig. 26c. BSE image of oldhamite in No. 504. The peripheral portion of oldhamite seems to have altered. A silicate aggregate (SL) consists mainly of enstatite and albite. Width is 68 μm .

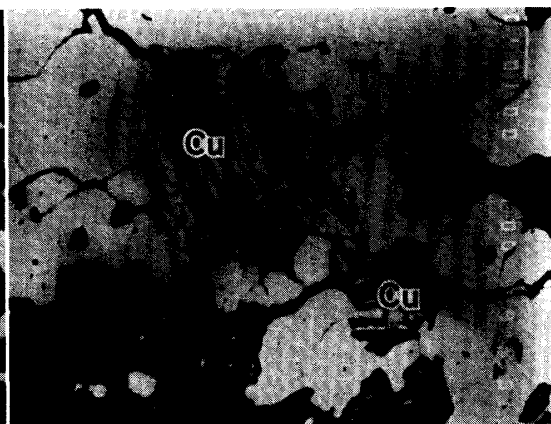


Fig. 26d. BSE image of a Cu-S-O phase (Cu) in No. 504. It shows a remarkable striped pattern. Width is 69 μm .

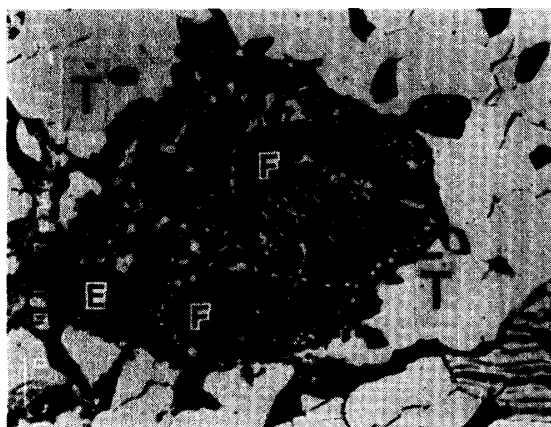


Fig. 26e. BSE image of a silicate aggregate in No. 504. It consists of forsterite and CaO-rich enstatite with minor troilite. Width is 100 μm .

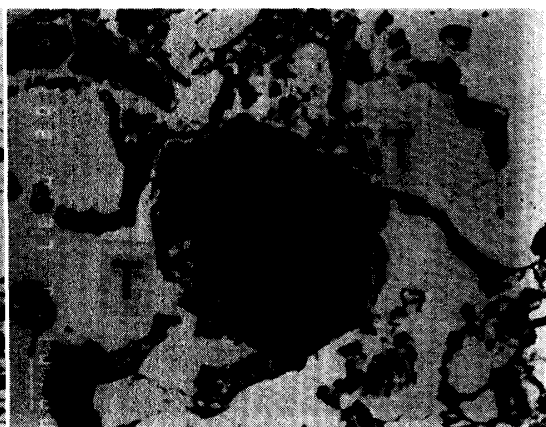


Fig. 26f. BSE image of CaO-poor enstatite in No. 504. Width is 105 μm .



Fig. 27a. Photomicrograph (ref. light) of No. 543. Djerfisherite is completely surrounded by porous troilite. A silicate aggregate (SL) is observed in the lower-left portion. Width is 300 μm .



Fig. 27b. BSE image of a silicate aggregate in No. 543. It consists of enstatite with minor amounts of albite and troilite. Albite occurs in interstitial spaces between enstatite. Width is 56 μm .

librium with a silica mineral, the equation obtained by LARIMER and BUSECK (1974) with Si=0.039 mol% (=2 wt%) gives the oxygen partial pressure of 4×10^{-23} atm at 1300 K, 10^{-29} atm at 1100 K, 10^{-39} atm at 900 K, and 3×10^{-54} atm at 700 K.

5.2. Perryite, $(Ni, Fe)_5(Si, P)_2$, and Schreibersite, $(Fe, Ni)_3P$

Perryite occurs commonly in association with kamacite and schreibersite in nodules. The chemical compositions are shown in Table 2. The atomic ratios of P/(P+Si) and Ni/(Ni+Fe) of perryite and the coexisting phases are plotted in Fig. 30 with those in EH chondrites and aubrites. The triangle of Y-691 is similar to that of Kota Kota (Fig. 30(a)). The Co content of perryite in Y-691 is low (0–0.08 wt%, Table 2) and the average Co/Ni wt% ratio is about 0.005.

Schreibersite occurs commonly as small rounded grains in kamacite, troilite or sphalerite. Schreibersite in troilite or sphalerite seems to be relic grains which had been left after the sulfurization of kamacite. The chemical compositions are shown in Table 3. The Co content of schreibersite is low (0–0.09 wt%, Table 3) and the average Co/Ni wt% ratio is about 0.01, which is higher than that of perryite (0.005) and lower than that of kamacite (0.16).

5.3. Troilite, FeS

Troilite occurs in almost all nodules in Y-691. Troilite in massive nodules shows two appearance; massive and porous (EL GORESY *et al.*, 1988). The latter includes many tiny pits, the size being less than a few micrometers (Figs. 14b, 14c, 15b, 17b,

Fig. 28. Ni-Si plot (wt%) of kamacites. (a) Y-691; (b) EH chondrites (open circles), EL chondrites (solid circles) and aubrites (open triangles). Data sources: KEIL and ANDERSEN (1965), WASSON and WAI (1970), RAMBALDI and RAJAN (1983), RUBIN (1983, 1984), SEARS and WEEKS (1984), and PRINZ *et al.* (1984).

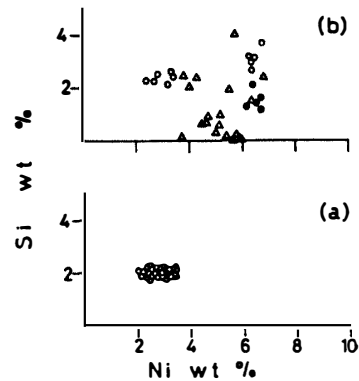


Fig. 29. Ni-Co plot (wt%) of kamacites. (a) Y-691; (b) Symbols are the same as those in Fig. 28(b). Data sources are the same as those in Fig. 28.

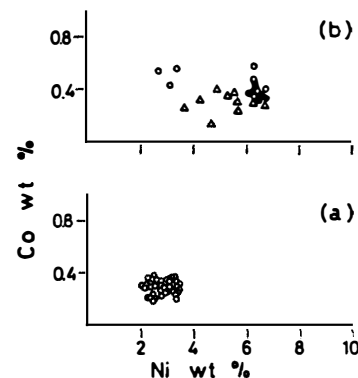


Table 2. The chemical compositions of perryites in Y-691.

1	2	3	4	5	6	7	8	9	10	11	12	13
1	500	500	505	507	508-I	508-I	511	513-I	528	528	539	539
2 Si	11.50	11.49	11.76	11.88	11.73	11.76	11.73	11.71	11.33	11.90	11.82	12.18
3 P	4.01	3.94	4.11	4.24	3.88	3.79	4.01	3.92	3.94	3.94	3.86	3.80
4 Cr	0.01	0.05	0.00	0.00	0.10	0.05	0.05	0.02	0.11	0.07	0.00	0.00
5 Fe	6.76	7.02	7.88	8.53	7.70	8.24	9.18	9.36	9.80	8.94	10.00	9.61
6 Co	0.05	0.02	0.00	0.08	0.01	0.04	0.08	0.01	0.00	0.00	0.00	0.08
7 Ni	79.18	78.08	77.40	75.96	77.97	76.61	75.65	76.16	75.70	76.11	74.70	75.71
8 Total	101.51	100.60	101.15	100.69	101.39	100.49	100.70	101.18	100.88	100.96	100.38	101.38

Table 3. The chemical compositions of schreibersites in Y-691.

1	2	3	4	5	6	7	8	9	10	11	12	13	14	15	16	17
1	500	500	501	503	503	503	503	505	506	507	507	509	509	509	510	513-I
2 Si	0.24	0.16	0.20	0.14	0.16	0.16	0.14	0.19	0.19	0.15	0.17	0.18	0.16	0.17	0.17	0.14
3 P	16.26	15.40	16.55	15.62	15.66	15.47	15.29	16.34	16.13	16.44	16.73	15.48	15.59	15.56	15.51	16.28
4 Cr	0.02	0.00	0.04	0.00	0.02	0.10	0.15	0.04	0.05	0.00	0.00	0.00	0.01	0.12	0.05	0.04
5 Fe	67.84	68.50	66.47	68.64	69.19	68.09	66.63	68.75	67.35	67.25	67.01	66.75	68.51	68.21	69.33	69.15
6 Co	0.09	0.05	0.00	0.04	0.12			0.00	0.00	0.06	0.00	0.01	0.07	0.00	0.03	0.01
7 Ni	17.08	15.93	16.49	16.78	16.51	16.34	18.71	15.96	17.91	17.59	17.71	18.35	15.57	16.06	15.22	16.20
8 Total	101.53	100.04	99.75	101.22	101.66	100.16	100.92	101.28	101.63	101.49	100.62	101.77	99.91	100.12	100.31	101.82

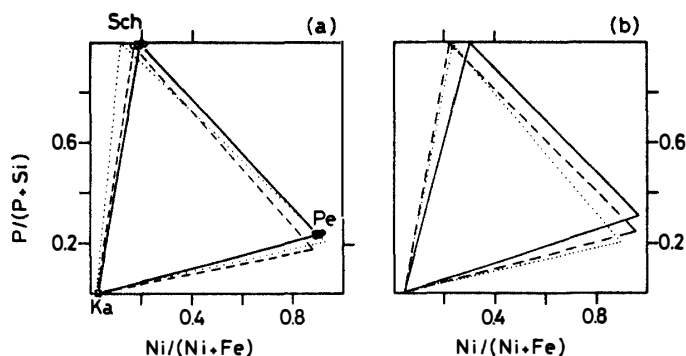


Fig. 30. The compositional relations among kamacite (Ka), schreibersite (Sch) and perryite (Pe). (a) E chondrites; Y-691 (kamacite—open squares, schreibersite—open circles, and perryite—solid circles), Kota Kota (solid line), Qingzhen (bar line), and Parsa (dot line). (b) aubrites; Norton County (solid line), Horse Creek (bar line), and Mt. Egerton (dot line). Data sources: WASSON and WAI (1970), RAMBALDI and RAJAN (1983) and PRINZ *et al.* (1984).

20b, 21b, 26b, and 27a), whereas the former never does. The massive troilite includes often thin daubreelite lamellae, and the original Cr contents of the massive troilite should have been higher than the present Cr contents. On the other hand, porous troilite never contains daubreelite lamellae. Troilite in concentric nodules is massive ones, and sometimes includes daubreelite lamellae.

The chemical compositions of troilite are shown in Table 4. Troilite in Y-691 contains small and variable amounts of Cr, and the Cr and Fe wt% of troilite in Y-691 are plotted in Fig. 31. Massive troilite is high in Cr contents, ranging from 0.6 to 2.4 wt%. On the other hand, porous troilite is lower in Cr contents, ranging from 1.2 to 0.05 wt%. However, the Cr content of porous troilite is nearly the same as that of massive troilite in a same nodule (Table 4). The Cr content of porous troilite in a Djer-Tr nodule No. 504 is the lowest among all troilites in Y-691 (Table 4), and porous troilite in Ka-Tr or Tr nodules are slightly higher in Cr contents than that in Djer-Tr nodules.

Although the chlorine content of massive troilite is nearly zero, that of porous troilite ranges from zero up to 8.2 wt% (Table 4). The Cl content is extremely heterogeneous in a porous troilite, changing by a few percents in a distance of a few microns. This means that the chlorine is included locally and is not in crystallographic lattice of troilite. The Cl content may be due to Cl-bearing tiny inclusions in the porous troilite. Although the Cl-bearing phase is not known, it can be $FeCl_2$ because the Cl-richest troilite (Column 59 in Table 4) contains excess Fe besides FeS component. Lawrencite was firstly found by KEIL (1968) in enstatite chondrites, but it is susceptible to terrestrial weathering.

5.4. Ninningerite, $(Mg, Fe)S$, and Oldhamite, CaS

Ninningerite in Y-691 occurs in many nodules and as isolated mineral fragments in the matrix. Chemical compositions of niningerite in Y-691 are shown in Table 5 and are plotted in Fig. 32 with those in EH and EL chondrites. Ninningerite in Y-691 is the richest in Mg content and the Fe and Mn contents are the lowest among all E

Table 4. The chemical compositions of troilites in Y-691. The abbreviations *m* and *p* are massive and porous troilites, respectively. The Cl content of porous troilites seems to be due to tiny inclusions of FeCl₂ or its altered products.

	1	2	3	4	5	6	7	8	9	10	11	12	13	14	15
1		500	500	501	501	501	501	502-I	503	503	503	503	504	504	504
2		m	m	m	m	p	p	m	m	m	p	p	p	p	p
3 S		36.54	37.61	37.22	35.82	35.83	34.52	36.56	36.80	36.59	35.59	35.81	34.87	34.35	34.87
4 Cr		1.04	1.71	0.92	0.62	0.62	0.64	0.97	1.23	1.28	1.12	1.13	0.07	0.05	0.07
5 Fe		60.97	59.97	61.79	64.05	63.07	63.37	61.76	60.38	60.55	58.66	60.61	61.54	64.48	61.54
6 Ni		0.02	0.18	0.03				0.21	0.00						
7 Cl				0.00	0.00	0.33	1.28		0.00	0.00	4.54	0.66	1.60	0.84	1.60
8 Total		98.57	99.47	99.96	100.49	99.85	99.81	99.50	98.41	98.42	99.91	98.21	98.08	99.72	98.08

	16	17	18	19	20	21	22	23	24	25	26	27	28	29	30
1		504	504	505	506	506	506	508-I	509	509	512	512	513-I	516-II	517
2		p	p	m	p	p	p	m	m	p	m	m	m	m	m
3 S		37.21	37.62	37.80	35.57	36.07	37.27	37.39	36.58	33.39	36.68	36.50	36.60	36.54	34.95
4 Cr		0.26	0.20	1.05	0.28	0.21	0.62	1.15	0.97	1.14	0.65	0.68	1.91	1.67	0.94
5 Fe		63.06	62.88	60.89	62.22	63.68	61.18	60.63	62.21	61.53	61.16	61.79	59.47	60.70	62.48
6 Ni		0.08	0.05	0.02			0.00	0.66	0.13		0.02	0.11	0.13	0.00	0.00
7 Cl		0.00	0.00		1.12	0.10	0.51		0.00	2.71					
8 Total		100.61	100.75	99.76	99.19	100.06	99.58	99.83	99.89	98.77	98.51	99.08	98.11	98.91	98.37

Table 4. (continued).

	31	32	33	34	35	36	37	38	39	40	41	42	43	44	45
1		520	520	528	528	529	529	530	531	532	537	538	539	542	542
2		m	m	m	m	m	m	m	m	m	m	m	m	p	p
3 S		36.68	36.86	35.83	36.92	35.73	39.24	36.11	36.67	35.88	36.36	35.32	36.54	35.39	35.84
4 Cr		1.71	1.44	1.07	0.95	1.03	1.11	1.22	1.72	1.25	1.16	1.82	0.98	0.43	0.40
5 Fe		60.76	61.61	62.06	62.32	61.40	60.12	61.17	60.42	61.78	61.95	60.90	60.76	62.29	62.37
6 Ni		0.03	0.00	0.04	0.06	0.23	0.18	0.10	0.01	0.00	0.14	0.21	0.19	0.11	0.00
7 Cl															
8 Total		99.18	99.91	99.00	100.25	98.39	100.65	98.60	98.82	98.91	99.61	98.25	98.47	98.22	98.61

	46	47	48	49	50	51	52	53	54	55	56	57	58	59	60
1		543	543	545	546	547	548	548	549	550	601	601	601	601	602
2		p	p	p	m	m	m	m	m	m	p	p	p	p	m
3 S		37.17	35.62	35.31	36.62	36.47	36.75	36.43	35.66	36.81	36.59	35.87	35.45	30.42	36.40
4 Cr		0.34	0.27	0.21	1.06	1.13	1.10	1.11	1.06	1.07	0.18	0.13	0.29	0.25	2.33
5 Fe		63.82	61.54	61.81	60.87	61.08	62.65	60.75	63.03	61.21	61.44	64.95	61.01	57.35	59.17
6 Ni		0.00		0.05	0.20	0.00	0.00	0.00	0.08	0.15	0.07				0.00
7 Cl			1.91								0.31	0.80	1.32	8.24	
8 Total		101.33	99.34	97.38	98.75	98.68	100.50	98.29	99.83	99.24	98.59	101.75	98.07	96.26	97.90

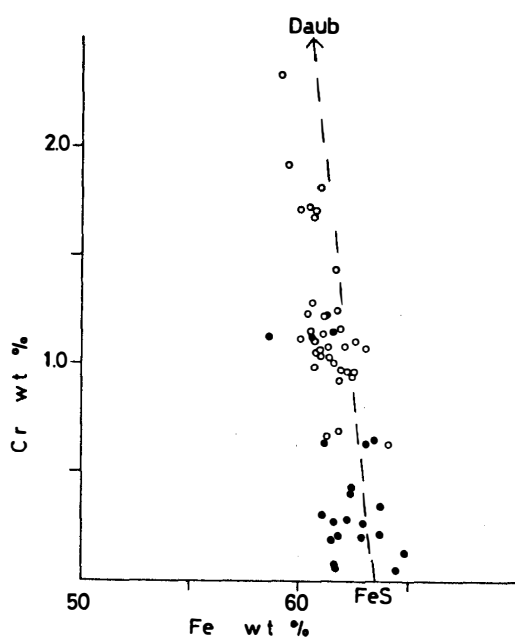


Fig. 31. Fe-Cr plot (wt%) of massive (open circles) and porous (closed circles) troilites in Y-691. The tie line between FeS and daubreelite (Daub) is partly shown by a bar line.

chondrites. Considering the extrapolation of isotherms (SKINNER and LUCE, 1971) shown in Fig. 32, the Y-691 niningerite can coexist with troilite at the temperatures lower than 600°C. The Ca/(Mg+Ca+Mn+Fe) atomic ratios of niningerites in Y-691 range from 0.004 to 0.012, and the geothermometer of CaS contents in niningerite by SKINNER and LUCE (1971) gives the temperatures from 400 to 550°C. In a concentric nodule No. 528, the core consists of niningerite, which includes a large troilite crystal in the central portion (Fig. 9a). The elongation of the large troilite is the same as one orientation of the troilite exsolution lamellae occurring in niningerite (Fig. 9b). The large troilite itself may have been produced by exsolution from FeS-rich niningerite.

The low Mn contents of niningerite in Y-691 may be explained by the following two reasons: a larger amount of Mg occurs as MgS in Y-691 and the Mn content in niningerite was diluted. Further, the Mn content of Y-691 whole rock (SHIMA and SHIMA, 1975) is the lowest among EH chondrites.

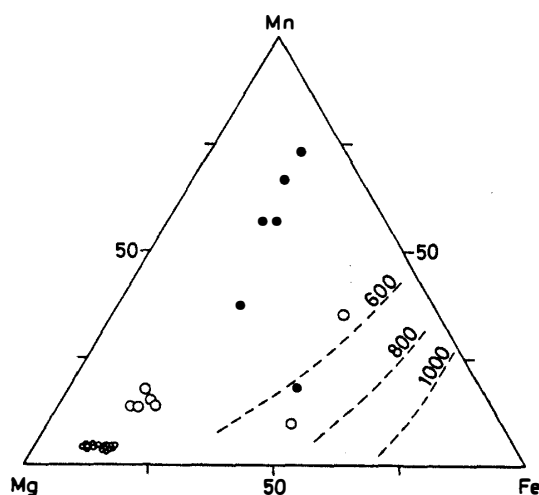


Fig. 32. Mg-Fe-Mn plot (atomic) of niningerite and alabandite in Y-691 (small open circles), EH chondrites (large open circles) and EL chondrites (solid circles). The solubility limits of niningerite-alabandite solid solution against troilite (FeS) at the temperatures of 600°, 800°, and 1000°C are shown (SKINNER and LUCE, 1971). Data sources: KEIL and ANDERSEN (1965), RAMBALDI and RAJAN (1983), RUBIN (1984), and PRINZ et al. (1984).

Table 5. The chemical compositions of niningerites in Y-691.

	1	2	3	4	5	6	7	8	9	10	11	12	13
1	501	501	501	501	504	504	504	504	507	507	507	507	509
2 Mg	34.62	33.78	31.15	31.15	31.40	33.38	32.94	32.29	35.26	34.51	34.71	34.84	34.50
3 S	51.96	51.15	50.80	50.80	50.92	51.32	50.38	49.45	50.02	50.75	50.49	51.14	51.16
4 Ca	0.26	0.33	0.40	0.40	0.38	0.28	0.40	0.40	0.32	0.32	0.34	0.31	0.27
5 Cr	0.15	0.09	0.16	0.16	0.17	0.06	0.13	0.07	0.10	0.15	0.13	0.09	0.09
6 Mn	3.62	4.35	4.27	4.27	3.87	2.10	3.60	2.89	4.06	4.15	4.04	3.93	3.17
7 Fe	11.10	11.81	13.08	13.08	11.66	14.08	13.63	13.66	9.73	10.47	9.30	9.06	10.02
8 Ni	0.00	0.02	0.06	0.06	0.06	0.00	0.00	0.02	0.02	0.00	0.00	0.00	0.07
9 Total	101.71	101.53	99.92	99.92	98.46	101.22	101.08	98.78	99.51	100.35	99.01	99.37	99.28

	14	15	16	17	18	19	20	21	22	23	24	25	26
1	510	512	512	512	512	512	521	527	528	537	538	538	548
2 Mg	35.01	32.07	31.81	31.81	31.97	31.91	31.07	31.74	32.53	31.52	32.22	31.51	30.79
3 S	51.90	49.60	49.96	49.96	49.20	49.39	51.09	50.16	50.84	49.04	49.27	51.45	49.25
4 Ca	0.35	0.33	0.34	0.34	0.33	0.39	0.74	0.58	0.38	0.38	0.38	0.33	0.43
5 Cr	0.14	0.12	0.10	0.10	0.12	0.09			0.17	0.12	0.13	0.10	0.35
6 Mn	4.58	4.06	4.15	4.15	3.38	3.91	3.64	3.50	4.17	5.03	4.90	4.53	4.90
7 Fe	9.19	13.23	12.48	12.48	14.16	13.63	12.07	13.06	12.65	13.83	13.01	13.68	13.84
8 Ni	0.01	0.06	0.01	0.01	0.07	0.12			0.13	0.16	0.05	0.06	0.08
9 Total	101.18	99.47	98.85	98.85	99.23	99.44	98.61	99.04	100.87	100.08	99.96	101.66	99.64

Y-691 Chondrite (E3) IV

Table 6. The chemical compositions of oldhamites in Y-691.

	1	2	3	4	5	6	7	8	9	10	11	12	13	14
1		504	504	504	504	521	521	521	521	521	522	522	522	527
2 Mg		0.35	0.50	0.40	0.43	0.32	0.49	0.42	0.40	0.37	0.33	0.37	0.41	0.44
3 S		44.05	43.90	42.76	45.18	45.33	44.98	44.07	44.99	44.56	44.97	45.11	44.45	43.37
4 Ca		53.34	55.07	53.80	53.49	54.72	52.50	54.23	53.12	53.07	53.46	54.63	53.31	54.63
5 Mn		0.19	0.11	0.36	0.38	0.19	0.25	0.19	0.06	0.22	0.08	0.06	0.14	0.33
6 Fe		0.89	0.41	1.02	0.83	0.17	0.37	0.35	0.21	0.65	0.80	0.37	0.51	0.28
7 Total		98.82	99.99	98.34	100.31	100.73	98.59	99.26	98.78	98.87	99.64	100.54	98.82	99.05

Table 7. The chemical compositions of sphalerites in Y-691.

	1	2	3	4	5	6	7	8	9	10	11
1		500	514	514	516-II	516-II	516-II	516-II	517	518	519
2 Mg		0.48	0.71	0.71	0.99	0.77	0.61	1.04	0.80	0.67	1.00
3 S		35.22	35.24	34.84	36.05	34.02	35.42	35.76	34.69	34.64	35.54
4 Cr		0.24	0.07	0.00	0.00	0.00	0.28	0.00	0.09	0.24	0.09
5 Mn		6.18	0.98	1.07	1.05	1.17	1.03	1.22	1.03	1.14	2.23
6 Fe		32.64	29.85	27.75	29.65	30.45	31.24	28.16	29.81	32.49	27.19
7 Ni		0.44	0.07	0.01	0.10	0.18	0.13	0.31	0.18	0.31	0.00
8 Cu		1.03	0.04	0.07	0.00	0.04	0.05	0.21	0.17	0.14	0.16
9 Zn		21.86	32.60	33.92	31.75	32.97	29.79	33.14	32.28	29.42	32.38
10 Total		98.09	99.56	98.37	99.59	99.60	98.55	99.84	99.05	99.05	98.59

Oldhamite in Y-691 occurs as small grains in nodules and as isolated mineral fragments. The chemical compositions are shown in Table 6. The peripheral portions of oldhamite are always altered (Fig. 26c). Fresh oldhamite shows a remarkable light-blue fluorescence under an electron beam of an EPMA, but altered one does not. Most oldhamite seems to have suffered from terrestrial alteration. The chemical composition of fresh oldhamite in Y-691 is nearly pure CaS. The $Mg/(Mg+Ca+Mn+Fe)$ and $Mn/(Mg+Ca+Mn+Fe)$ ratios of oldhamite in Y-691 are 0.010–0.015 and 0.0008–0.005, respectively, and the geothermometers by SKINNER and LUCE (1971) give the temperatures between 600 and 700°C.

5.5. Sphalerite, $(Zn, Fe)S$

Chemical compositions of sphalerite in Y-691 are shown in Table 7 and are plotted in Fig. 33. Most sphalerite in Y-691 are plotted in the range of FeS mol% from 55 to 47 and are similar to those in Qingzhen, although a sphalerite grain in the hexagon-shaped inclusion of No. 500 contains high Mn (6.2 wt%) and Cu (1.0 wt%) contents.

5.6. Djerfisherite, $(K, Na)_3(Cu, Ni)(Fe, Ni)_{12}S_{14}$

Djerfisherite occurs as small grains in Ka-Tr nodules and as a main phase in Djer-Tr nodules. Chemical compositions of djerfisherite are shown in Table 8 and are plotted in Fig. 34, showing that the Cu contents vary among nodules. Djerfisherite in No. 504, which includes a minor amount of a Cu-bearing phase (Fig. 26d), is the

Fig. 33. Fe-Zn-Mn plot (atomic) of sphalerites in Y-691 (open circles) and Qingzhen (solid circles, EL GORESY et al., 1988).

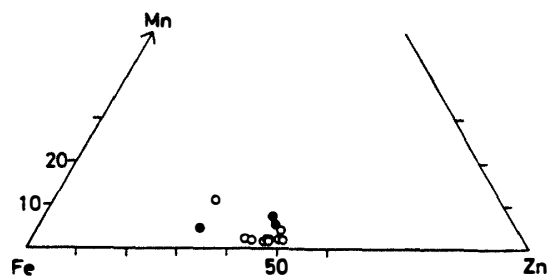
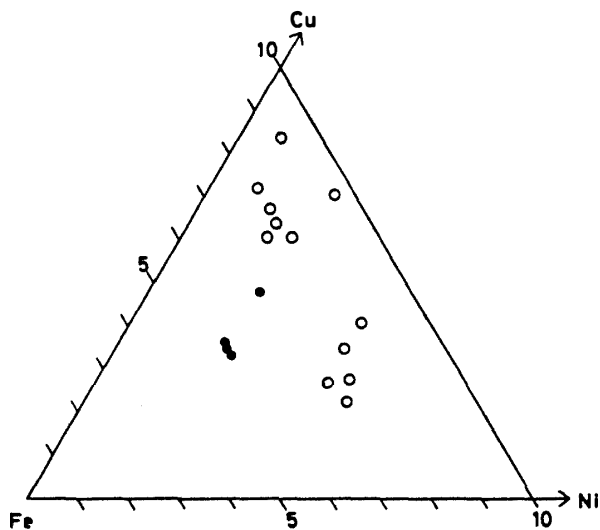


Fig. 34. Fe-rich portion of the Fe-Ni-Cu plot (atomic) for djerfisherites in Y-691 (open circles) and Qingzhen (solid circles, EL GORESY et al., 1988).



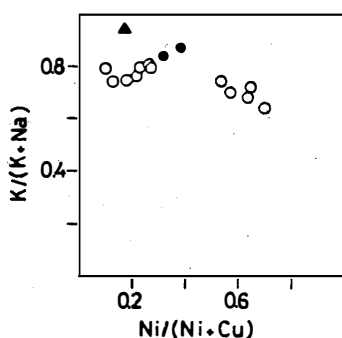


Fig. 35. The atomic ratios of K and Na of djerfisherites in Y-691 (open circles), Qingzhen (solid circles, EL GORESY *et al.*, 1988), and St. Marks (solid triangle, FUCHS, 1966) are plotted against the atomic ratios of Ni and Cu.

lowest in Cu content. In comparison to those in Qingzhen, djerfisherite in Y-691 enriches in Cu and Ni (Fig. 34). The K/(Na+K) ratio of djerfisherite in Y-691 is nearly constant at about 0.65–0.80 (Fig. 35). Djerfisherite is always surrounded by porous troilite (Figs. 14b, 26a and 27a), and that in No. 504 includes lamellae of porous troilite (Fig. 26b). Chlorine content of djerfisherite is 1.5–1.7 wt% (Table 8), and according to FUCHS (1966) its detection may have resulted from unobserved traces of lawrencite.

5.7. Cu-S-O phase

In a djerfisherite nodule No. 504, a Cu-S-O phase occurs as small inclusions (Fig. 26b) and shows a characteristic striped pattern (Fig. 26d). It shows heterogeneous chemical compositions including variable but minor amounts of Ca and Mg, and the oxygen content is also variable although it is a major component of Cu-S-O phase. However, the atomic ratio of Cu/S of the phase is always two, suggesting that the phase was originally chalcocite (Cu_2S) or digenite (Cu_9S_5) and it has been altered to oxygen-bearing phase by terrestrial weathering.

5.8. Caswellsilverite, NaCrS_2

Na-Cr-S phases occur as small inclusions in nodules of Y-691. However, the Na content varies continuously from about 15 wt% to less than 3 wt% among grains or in a grain, although atomic ratios of S to Cr are nearly 2 in spite of the low Na content, and a Na-Cr-S grain having the highest Na content gives a stoichiometric composition of caswellsilverite. Na-Cr-S phases having lower Na content may be altered products of caswellsilverite by terrestrial weathering. The chemical composition of fresh caswellsilverite is shown in Table 8 and is nearly pure NaCrS_2 .

5.9. Silicates in opaque-mineral nodules

Silicates in nodules are forsterite, enstatite, silica mineral, albite and roedderite. Enstatite and silica mineral are common silicates in nodules, and roedderite, forsterite and albite are minor. The chemical compositions are shown in Table 9.

Roedderite, $(\text{K}, \text{Na})_2(\text{Mg}, \text{Fe})_5\text{Si}_{12}\text{O}_{30}$, occurs as small euhedral grains included in niningerite or troilite (Figs. 1a, 23b, 24, and 25). The chemical composition is similar to that of roedderite in Indarch although the *mg* values are slightly higher, ranging from 0.97 to 0.99 (Fig. 36).

Enstatites in nodules occur as euhedral crystals (Fig. 23a), as rounded enstatite

Table 8. The chemical compositions of djerfisherites (Columns 2-12) and caswellsilverite (Column 13) in Y-691.

1	2	3	4	5	6	7	8	9	10	11	12	13
1	503	504	504	504	504	542	542	542	543	543	545	508-I
2 Na	2.14	1.71	1.47	1.83	2.13	1.52	1.17	1.42	1.12	1.61	1.12	15.31
3 S	33.27	34.68	35.73	35.53	35.30	32.56	33.73	31.32	33.67	33.23	33.79	45.49
4 K	8.03	6.74	6.56	6.58	6.46	8.24	8.15	8.03	7.76	7.95	7.76	0.07
5 Cr	0.04	0.00	0.00	0.00	0.03	0.02	0.00	0.01	0.04	0.00	0.06	36.31
6 Mn	0.00	0.00	0.00	0.00	0.00	0.00	0.00	0.06	0.00	0.00	0.03	0.21
7 Fe	48.61	50.20	50.25	50.69	51.45	49.93	49.76	51.36	49.55	50.83	50.72	0.77
8 Ni	0.49	2.62	2.87	2.63	3.03	0.83	0.94	1.02	0.47	0.56	1.39	0.07
9 Cu	5.11	2.18	1.71	1.66	1.43	4.20	3.73	4.08	5.21	4.54	4.17	0.12
10 Cl	1.58	1.54	1.52						1.72			
11 Total	99.27	99.67	100.11	98.92	99.83	97.30	97.48	97.30	99.54	98.72	99.04	98.35

Table 9. The chemical compositions of silicates in opaque-mineral nodules of Y-691. The numbers at the top of each column are nodule-numbers. The abbreviations, En, Roed, Fo, Silica, and Ab, are enstatite, roedderite, forsterite, silica-mineral, and albite, respectively. The symbol mg is MgO/(MgO+FeO) molar ratios.

1	2	3	4	5	6	7	8	9	10	11	12	13	14	15	16	17
1 Y-691	502-II	502-II	504	504	504	504	504	504	504	504	504	504	504	504	504	504
2	Roed	Roed	Fo	Fo	Fo	En	En	En	En	En	En	En	En	En	En	Silica
3 SiO ₂	70.40	70.62	40.83	41.20	42.06	58.46	58.01	57.90	58.02	58.62	57.24	56.56	57.21	56.21	57.17	98.09
4 TiO ₂	0.03	0.00	0.00	0.00	0.00	0.00	0.09	0.08	0.00	0.00	0.00	0.00	0.10	0.15	0.21	0.04
5 Al ₂ O ₃	1.29	0.65	0.00	0.00	0.00	0.20	0.29	0.24	0.12	0.09	0.21	0.91	0.85	0.64	0.65	0.85
6 Cr ₂ O ₃	0.04	0.00	0.47	0.45	0.41	0.21	0.29	0.40	0.26	0.37	0.34	0.64	0.72	0.82	0.86	0.03
7 FeO	1.14	1.33	0.95	1.12	0.96	0.54	1.05	1.22	1.57	1.95	3.37	6.46	6.54	1.49	2.66	1.16
8 MnO	0.00	0.00	0.54	0.75	0.42	0.00	0.00	0.26	0.21	0.08	0.00	0.13	0.27	0.76	0.59	0.00
9 MgO	19.45	20.61	56.84	56.38	57.10	39.56	39.45	39.36	39.27	39.64	37.71	35.08	35.14	37.47	36.76	0.06
10 CaO	0.33	0.15	0.26	0.17	0.15	0.31	0.13	0.09	0.14	0.22	0.20	0.42	0.26	2.12	2.15	0.00
11 Na ₂ O	3.78	3.60	0.03	0.08	0.00	0.00	0.00	0.03	0.05	0.00	0.11	0.08	0.00	0.10	0.13	0.46
12 K ₂ O	2.77	3.43	0.00	0.03	0.00	0.00	0.00	0.00	0.00	0.00	0.00	0.00	0.00	0.00	0.04	0.00
13 Total	99.23	100.39	99.92	100.18	101.10	99.28	99.31	99.58	99.64	100.97	99.18	100.28	101.09	99.76	101.22	100.69
14 mg	0.97	0.97	0.99	0.99	0.99	0.99	0.99	0.98	0.98	0.97	0.95	0.91	0.91	0.98	0.96	

Table 9. (continued).

	18	19	20	21	22	23	24	25	26	27	28	29	30	31	32	33	34
1		507	507	512	513-I	513-I	513-I	516-I	516-I	524	530	530	531	531	531	532	534
2		Fo	En	En	En	En	Ab	Fo	En	En	Roed	Roed	En	En	Roed	Roed	Ab
3 SiO ₂	40.27	57.01	58.51	57.51	57.22	66.41	41.59	57.52	57.80	70.69	71.90	59.35	58.43	71.19	70.66	69.33	
4 TiO ₂	0.03	0.00	0.15	0.00	0.00	0.00	0.06	0.00	0.08	0.09	0.06	0.00	0.00	0.07	0.00	0.00	
5 Al ₂ O ₃	0.00	0.56	0.78	0.10	0.00	18.07	0.03	0.16	0.33	0.76	0.47	0.00	0.00	0.33	0.78	19.33	
6 Cr ₂ O ₃	0.24	0.01	0.16	0.08	0.00	0.04	0.12	0.40	0.32	0.03	0.00	0.00	0.03	0.14	0.09	—	
7 FeO	1.33	1.88	0.73	2.34	2.24	2.62	3.24	2.11	1.95	0.23	0.66	0.46	0.78	0.54	1.25	0.98	
8 MnO	0.31	0.00	0.33	0.29	0.08	0.14	0.09	0.11	0.19	0.00	0.00	0.00	0.15	0.00	0.05	—	
9 MgO	57.25	38.77	39.00	40.02	39.51	0.20	53.34	38.12	39.79	19.38	20.21	40.85	39.64	20.99	20.51	0.34	
10 CaO	0.06	0.65	0.63	0.50	0.04	0.18	0.51	0.17	0.36	0.67	0.00	0.03	0.08	0.08	0.00	0.04	
11 Na ₂ O	0.04	0.03	0.04	0.03	0.08	11.26	0.10	0.22	0.08	3.21	3.09	0.00	0.00	3.26	3.29	11.27	
12 K ₂ O	0.00	0.00	0.00	0.00	0.00	0.13	0.00	0.00	0.00	3.92	4.42	0.00	0.06	3.95	4.14	0.07	
13 Total	99.53	98.91	100.33	100.87	99.17	99.05	99.08	98.81	100.90	98.98	100.81	100.69	99.17	100.55	100.77	101.36	
14 mg	0.99	0.97	0.99	0.97	0.97		0.97	0.97	0.97	0.99	0.98	0.99	0.99	0.99	0.97		

	35	36	37	38	39	40	41	42	43	44	45	46	47	48
1		534	536	536	537	537	537	537	537	538	539	601	602	602
2		Ab	En	Ab	En	Ab	Ab	Ab	Silica	Ab	En	Silica	Ab	Ab
3 SiO ₂		69.31	59.19	66.68	58.34	68.36	70.58	68.06	99.09	70.56	57.88	97.73	68.59	68.13
4 TiO ₂		0.00	0.00	0.00	0.00	0.00	0.00	0.05	0.07	0.05	0.07	0.00	0.00	0.00
5 Al ₂ O ₃		18.88	0.34	21.52	0.14	18.79	19.17	18.98	0.21	18.93	0.60	0.08	18.90	18.85
6 Cr ₂ O ₃		0.00	0.39	0.05	0.05	0.00	0.00	0.05	0.04	0.04	—	0.04	0.00	0.00
7 FeO		0.56	1.36	1.04	1.51	0.75	0.70	1.29	1.66	1.23	1.99	0.60	0.88	0.60
8 MnO		0.00	0.37	0.14	0.08	0.12	0.00	0.00	0.00	0.00	0.00	0.00	0.00	0.00
9 MgO		0.08	39.58	0.60	39.95	0.12	0.06	0.51	0.00	0.16	37.88	0.68	0.00	0.00
10 CaO		0.00	0.38	0.30	0.07	0.06	0.00	0.00	0.04	0.00	0.61	0.07	0.00	0.00
11 Na ₂ O		11.33	0.04	10.96	0.08	10.71	10.72	11.14	0.10	10.94	0.15	0.04	11.59	11.46
12 K ₂ O		0.14	0.00	0.62	0.00	0.20	0.08	0.05	0.00	0.06	—	0.05	0.09	0.07
13 Total		100.30	101.65	101.91	100.22	99.11	101.31	100.13	101.21	101.97	99.18	99.29	100.05	99.11
14 mg			0.98		0.98						0.97			

Fig. 36. The atomic ratios of K and Na of roedderites in Y-691 (open circles) and Indarch (solid circle, FUCHS *et al.*, 1966) and merrihueite in Mezo-Madaras (solid square, DODD *et al.*, 1965) are plotted against the atomic ratios of Mg and Fe.

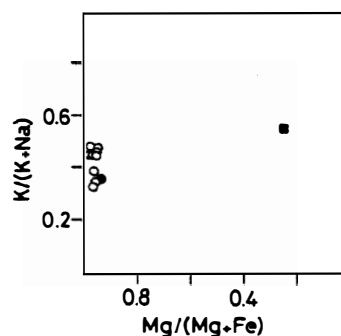
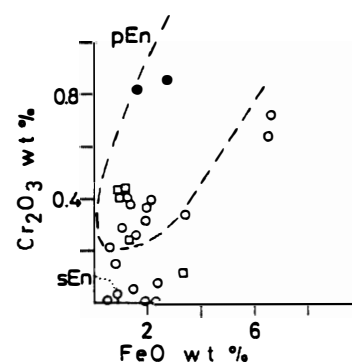


Fig. 37. $\text{FeO}-\text{Cr}_2\text{O}_3$ plot (wt%) of Ca-poor enstatite (open circles), Ca-rich enstatite (closed circles), and forsterite (open squares) in nodules. A bar line denoted by pEn and a dotted line denoted by sEn are compositional ranges of primary and secondary enstatites in Y-691 chondrules (IKEDA, 1989), respectively.



inclusions (Fig. 26f), as silicate aggregates (Figs. 15d, 26e and 27b), and as irregular grains in middle zones of concentric nodules (Figs. 1b, 2b, 4b and 5b). The *mg* values of enstatite except for that in a nodule No. 504 are more magnesian than 0.97, and the CaO content is lower than 0.65 wt%. Enstatites in No. 504 occur as rounded enstatite inclusions (Fig. 26f) and in a silicate aggregate (Fig. 26e). The *mg* value of enstatite in the rounded inclusions ranges from 0.91 to 0.99, being different among inclusion. The CaO content is lower than 0.5 wt%. On the other hand, an enstatite grain in the silicate aggregate is high in CaO (about 2.1 wt%) with the *mg* value of 0.96–0.98. The FeO and Cr_2O_3 contents of enstatite in nodules are shown in Fig. 37. Most of them are plotted in or near by the range of primary enstatite in Y-691 chondrules, and a few are plotted in the range of secondary enstatite (Fig. 37).

Forsterites in nodules occur in silicate aggregates of massive nodules (Fig. 15d) and in middle zones of concentric nodules (Figs. 2b and 5b). Sometimes forsterite occurs with a silica mineral in a same nodule, indicating that they were not in equilibrium. Forsterite never shows euhedral forms in nodules, and the *mg* value ranges from 0.97 to 1.00.

Silica minerals in nodules occur as silica-mineral blebs in troilite (Fig. 23b), in silicate aggregates (Figs. 15d and 23b), and in middle zones of concentric nodules (Figs. 1b, 2b and 5b).

Albites in nodules occur as albite inclusions (Figs. 7, 12b, 13b and 23a) and as silicate aggregates (Figs. 26c and 27b). It always associates with a silica mineral, enstatite, and/or sulfides. Albite are close in chemical composition to pure $\text{NaSi}_3\text{AlO}_8$, which is similar in chemical composition to secondary albite in chondrules and unusual silicate-inclusions (IKEDA, 1988b, 1989).

6. Discussion

6.1. Formation of kamacite

A hexagon-shaped inclusion occurs in a kamacite nodule No. 500 (Fig. 11b), and the formation of the hexagon may be explained by the following hypotheses; the hexagon was produced as a residual Fe-S melt pocket surrounded completely by cubic crystallographic planes of kamacite which crystallized as a liquidus phase. The other possibility is that a euhedral crystal of hexagonal pyrrhotite was later surrounded by Fe-metal precipitating from a gaseous or liquid phase. The former hypothesis seems to be preferable, because the hexagon is produced not only by troilite but also by schreibersite and because troilite in the inclusion is polycrystals (Fig. 11b). If so, kamacite in the nodule No. 500 is a product of crystallization of Fe melt, and the residual melt was enriched in S, P, Si, Ca and Zn to crystallize troilite, schreibersite, perryite, oldhamite, and sphalerite as the latest-stage phases. Most kamacites in massive nodules may have been formed in the same way as that in No. 500.

On the other hand, kamacites in concentric nodules seem to have a complex genesis. The core of concentric nodules shows an irregular outline, and the mineral assemblage of the core is similar to those of Ka and Ka-Tr subtypes of massive nodules, suggesting that the core may be a fragment of massive nodules. The mantle of concentric nodules are mainly kamacite, which formed after the attachment of disequilibrium silicates in the middle zones. The mantle kamacite may have precipitated directly from gaseous phases rather than by crystallization from Fe melts. The Si, P and Ni contents of kamacite are not different between the core kamacites and the mantle kamacites, although they could be originally different from each other (Table 1). The Si, P and Ni contents of kamacites are controlled by subsolidus precipitation of perryite and schreibersite from Fe metals saturated with Si, P and Ni contents, as shown in Fig. 30.

6.2. Formation of perryite and schreibersite

Schreibersite occurs in the hexagon-shaped inclusion of No. 500, and it may have crystallized along with Cr-rich troilite from the residual Fe-P-S melt. In addition to this, schreibersite occurs as small rounded grains in kamacite of many nodules without troilite, and these schreibersite may be due to exsolution from P-saturated Fe-metal. Perryite occurs partly in the hexagon-shaped inclusion of No. 500 and is partly surrounds the hexagon-shaped inclusion. The former may be a latest-stage product of the residual Fe-P-S melt, and the latter may be to exsolution from the Si-Ni-saturated Fe metal at subsolidus conditions. Perryite occurs also as irregular small grains in kamacite of many nodules, and it may be due to exsolution.

6.3. Formation of troilite and daubreelite

As already stated, troilite in the hexagon-shaped inclusion of No. 500 is the latest-stage product of crystallization from a residual Fe-P-S melt. Therefore, some massive troilite may have crystallized from Fe-S melts. However, other massive troilite and porous troilite show a replacement texture (Figs. 14b, 14c, 15b, and 17b); the shape and size of perryite and schreibersite in massive and porous troilites are

similar to those in neighbouring kamacite, suggesting that the perryite and schreibersite in the troilite are relic after the sulfurization of kamacite by H_2S -bearing gases. These massive and porous troilites may have been formed from kamacite by sulfurization under subsolidus conditions.

As already stated in Section 5.3, the Cr content of porous troilite is nearly the same as that of massive troilite in a same nodule, and the remarkable difference in chemical composition between porous and massive troilites is chlorine content (Table 4). Porous troilite seems to include many tiny $FeCl_2$ inclusions, the size being less than a few micrometers. The $FeCl_2$ may have been formed during sulfurization of kamacite at the same time as the host troilite. The porous texture may be due to the remnant of tiny $FeCl_2$ inclusions which have been reacted with terrestrial water during or after the thin section preparation.

The third genesis of troilite is exsolution lamellae which are observed in niningerite (Fig. 6a). Lamellae of porous troilite in djerfisherite (Fig. 26b) could be due to fracture-filling rather than exsolution.

Daubreelite occurs as exsolution lamellae in massive troilite, which contains Cr more than 0.9 wt%. EL GORESY and KULLERUD (1969) showed that two assemblages of (Cr-rich pyrrhotite+daubreelite+CrS) and (Cr-rich pyrrhotite+Fe-metal+CrS) are stable at the temperature of 700°C and that an assemblage of (Cr-rich pyrrhotite+Fe-metal+daubreelite) is stable at the temperature of 600°C. This indicates that daubreelite in Y-691 was produced from Cr-rich pyrrhotite (or troilite) as exsolution lamellae at the temperature lower than 600–700°C.

6.1. Formation of sphalerite and Cu-sulfide

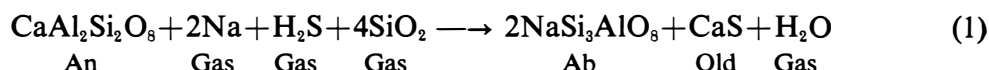
Sphalerite is observed in the hexagon-shaped inclusion of No. 500 and may be a product of crystallization from a residual Fe-P-S melt. On the other hand, sphalerite in a Ka-Nin nodule No. 516-II (Fig. 19a) is a large grain up to about 100 microns in length and seems not to be a product of crystallization from a Fe-P-S melt. The sphalerite includes small rounded schreibersite grains which are similar in shape and size to those in the neighbouring kamacite (Fig. 19b). The occurrence of the sphalerite suggests that it was produced by replacement of kamacite with a gaseous phase. A small sphalerite grain occurs in porous troilite (Figs. 20b and 21b), and it shows a porous texture similar to that of the host troilite, suggesting that the sphalerite had been formed along with the host troilite during sulfurization of kamacite, including tiny $FeCl_2$ inclusions.

BOORMAN (1967) and BARTON and TOULMIN (1966) showed that the sphalerite containing about 50 mol% FeS coexists with Fe metal and pyrrhotite (or troilite) in a wide temperature range from 900° to 300°C. HUTCHISON and SCOTT (1983) presented a sphalerite cosmobarometer, and the barometer with $P=0$ kb and FeS=50 mol% gives $T=472^\circ C$.

Cu-sulfide (chalcocite or digenite) are not observed in Y-691, but the altered products of chalcocite or digenite are observed to be included in Djer-Tr nodules (Fig. 15c). Chalcocite or digenite is stable in a Cu-S system at wide temperatures lower than 1100°C or 900°C, respectively (KULLERUD, 1958).

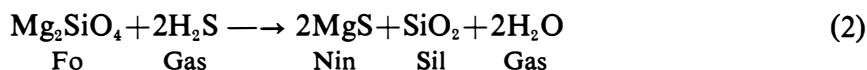
6.5. Formation of oldhamite and niningerite

The atomic ratios of Ca/Al of Y-691 chondrules are variable (IKEDA, 1988a) and are systematically lower for the SP chondrules (the Al/(Al+Na) ratios smaller than 0.65) than the IP and CP chondrules (larger than 0.65) (IKEDA, 1989). This suggests that the precursors of the SP chondrules depleted in Ca relative to Al. The depletion of Ca is explained by the following reaction;



The anorthite (An) component in the chondrule precursors changes to albite (Ab) component, and the oldhamite (Old) component in the right hand side of eq. (1) separates from the precursors of SP chondrules to be included in opaque-mineral nodules. In some nodules, oldhamite occurs in association with albite (Fig. 12b).

In a nodule No. 501, niningerite includes small rounded schreibersite grains (Fig. 15c), which are also included in the neighbouring kamacite. This suggests that some niningerite was produced by replacement of kamacite and the FeS component of niningerite may be supplied by sulfurization of Fe metal. However, it is difficult to clarify the origin of MgS component of niningerite. Considering that forsterite in nodules seems to be unstable (Figs. 2b, 5b, 15d, and 26e) and that niningerite occurs often with a silica-mineral and/or enstatite in nodules (Figs. 1b and 4b), possible reactions to form MgS component are:



and/or



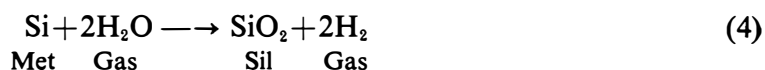
6.6. Origin of olivine, pyroxene and silica mineral in nodules

Pyroxene in some nodules shows a wide range of *mg* values in nodules, and sometimes olivine occurs together with a silica mineral in a nodule. These facts indicate that olivine, pyroxene and a silica mineral in nodules were not in equilibrium. The FeO-Cr₂O₃ correlation of pyroxenes and olivines in most nodules are similar to those in chondrules in Y-691 (Fig. 37). The CaO content of enstatite in nodules is lower than 0.7 wt% except for CaO-rich enstatite (CaO=2.1–2.2 wt%) in a silicate-aggregate of No. 504. The CaO content of primary enstatite in porphyritic, granular and radial-Px chondrules of Y-691 is lower than 0.7 wt%, and that of primary enstatite in barred-Ol chondrules ranges from 1.5 to 3.0 wt% (IKEDA, 1989). On the other hand, FeO, Cr₂O₃ and CaO contents of secondary enstatite in Y-691 chondrules are lower than 0.1, 0.8, and 0.1 wt%, respectively (IKEDA, 1989). Therefore, enstatite in most nodules is similar in chemical composition to primary enstatite in chondrules with a few exceptions, suggesting that pyroxene and probably olivine in nodules may have been supplied from chondrules by disaggregation in the protosolar nebula.

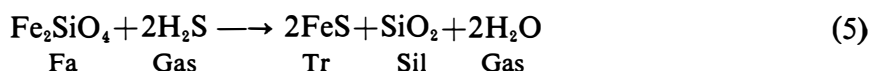
However, enstatite in nodules Nos. 531 and 601 shows euhedral forms (Figs. 21b and 23a), and they seem not to be fragments of chondrule pyroxene. The FeO,

Cr₂O₃, and CaO of enstatite in No. 531 are 0.4–0.8, 0.00–0.03, and 0.03–0.08 wt%, respectively, being similar to those of secondary enstatite in chondrules. These euhedral enstatite in nodules may have been formed as a direct condensate from a reduced gas by eq. (3), or by a reaction of Mg₂SiO₄ with SiO₂ component in a reduced gas.

A silica mineral in nodules may have four geneses: first is disaggregation of silica-mineral-bearing chondrules, the second is direct precipitation by fractional condensation from a reduced gas, and the third is oxidation of a metallic Si component in Fe metals;



where Met and Sil are a metallic component in kamacite and a silica mineral, respectively. Especially, reaction (4) may easily proceed during sulfurization of the host kamacite to produce troilite. The last possible reaction to produce silica minerals is eq. (2) or a reaction similar to eq. (2);



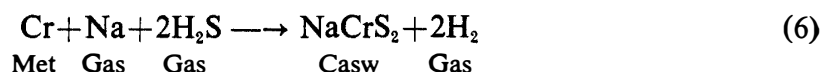
where Fa and Tr are fayalite component of olivine and troilite, respectively.

Silica mineral in No. 502-II (Fig. 1b) can have been produced by eq. (2), that in a silicate-aggregate of No. 501 (Fig. 15d) by eq. (5), and that in a middle zone of No. 511 (Fig. 3) by eq. (4) or by direct condensation. An example of reaction (4) which took place during sulfurization may be blebs of silica mineral included in troilite (Fig. 23b).

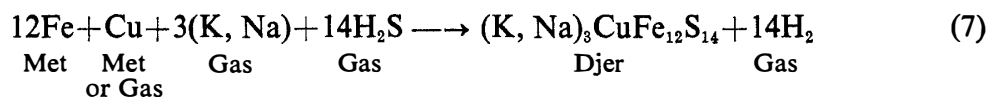
6.7. Formation of alkali-bearing phases

The alkali-bearing phases in nodules of Y-691 are albite, caswellsilverite, roederite and djerfisherite.

According to equilibrium condensation theory (LARIMER, 1967; GROSSMAN and LARIMER, 1974; FEGLEY and LEWIS, 1980; SAXENA and ERIKSSON, 1983), high-temperature condensates contain Al and are free from alkalies which remain in the nebular gas. With decreasing temperatures the Al-bearing high-temperature condensates react with a Na-bearing nebular gas to produce albite component consuming anorthite component at the temperatures lower than 1100°C under the total gas pressure of 10⁻⁴ atm. However, the case is not true when fractional condensation takes place; if the Al-bearing high-temperature condensates separate from the reaction system, the Na-bearing gas can not produce albite component at the temperatures lower than 1100°C because of lacking of Al in the reaction system. In such a case, Na₂S and K₂S condense instead of albite (FEGLEY and LEWIS, 1980). However, Na₂S and K₂S are not observed in Y-691. Instead of them, alkali-bearing sulfides, caswellsilverite and djerfisherite, occur in Y-691 nodules. The possible reactions to produce caswellsilverite and djerfisherite are:

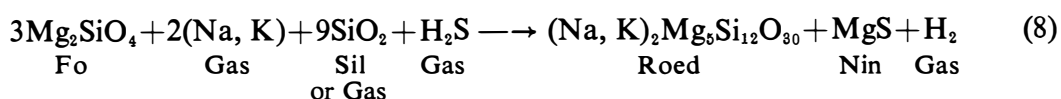


and



where Met, Casw and Djer are metallic component in kamacite, caswellsilverite and djerfisherite, respectively. Djerfisherite in Y-691 always contains Ni (Table 8) and the atomic ratios of Ni/Fe are similar to those of kamacite in Y-691 (Table 1), supporting that the main reaction to produce djerfisherite is eq. (7).

Roedderite in Y-691 occurs included by niningerite or troilite. A possible reaction to produce roedderite is;



The reaction (8) is supported by the intimate association of roedderite and niningerite in nodules of Y-691 (Figs. 1a and 25).

Figure 38 shows the compositional relationship among alkali-bearing phases in Y-691. A high-temperature gas having Al, Na and K contents of the solar system elemental abundances (CAMERON, 1973) is assumed; when the fractional condensation takes place incompletely with decreasing temperatures, the gas enriches in alkalis, and the alkalis in the gas react with minor anorthite remaining in the reaction system to produce albite by the reaction (1). However, all alkalis in the gas can not condense as albite because most fractions of Al had already been separated from the reaction system by fractionation. With subsequent decrease in temperature, the remaining alkalis in the gas condense as caswellsilverite and roedderite according to the reactions (6) and (8). After consuming the most Na by forming albite, caswellsilverite and roedderite, the gas enriches in K and finally djerfisherite condense by the reaction (7) in a low temperature range.

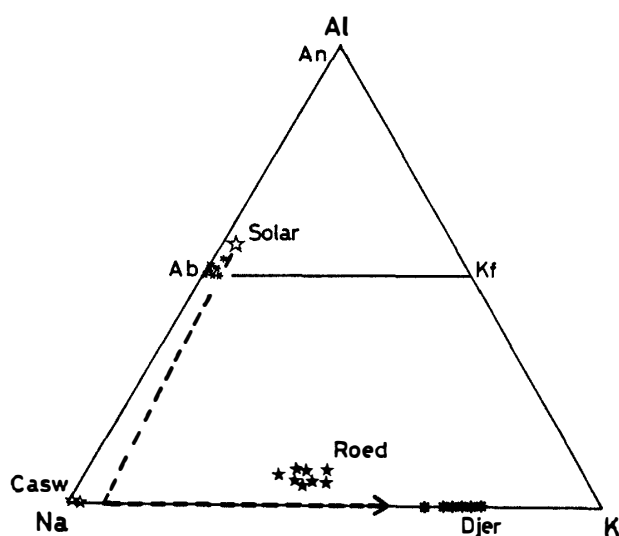


Fig. 38. Na-K-Al plot (atomic) of alkali-bearing phases in Y-691 nodules. Albite (Ab, small asterisks), caswellsilverite (Cas, small open stars), roedderite (Roed, solid stars), and djerfisherite (Djer, large asterisks). The abbreviations, An, Kf and Solar, are anorthite, K-feldspar and solar system elemental abundances (a large open star, CAMERON, 1973), respectively.

6.8. *Metamorphism after the accretion*

Any effect of thermal metamorphism after the accretion is not detected petrographically in Y-691 nodules. Chondrules in Y-691 also did not suffer from thermal metamorphism after the accretion (IKEDA, 1989). However, EL GORESY *et al.* (1988) suggested that metamorphic events took place in the Y-691 parent body at 800 Ma ago (MULLER and JESSBERGER, 1985) and that djerfisherite decomposed to porous troilite and other sulfides by the thermal reactions. As already stated, djerfisherite grains in Y-691 are completely surrounded by porous troilite (Figs. 14b, 26a, 26b, and 27a), and the reaction of djerfisherite with a fluid phase to produce porous troilite is plausible. However, the Cr content of porous troilite is nearly the same as that of massive ones in a same nodule, and it varies among nodules, although the Cr content of djerfisherite in Y-691 nodules is nearly zero (Table 8). This suggests that porous troilite was produced in a similar condition to the coexisting massive troilite, and it is likely that the massive troilite was firstly produced from kamacite by sulfurization and in the subsequent stage porous troilite was produced along with lawrencite from kamacite by sulfurization or by reaction of djerfisherite with the ambient nebular gas. If the sulfurization of kamacite or reaction of djerfisherite to produce porous troilite took place at a lowest temperature in the nebula, porous troilite containing the lowest Cr content may have been formed. Further work on the apparent young Ar-Ar age of Y-691 (HONDA *et al.*, 1983; MULLER and JESSBERGER, 1985) should be done.

7. Summary

Several kinds of constituent minerals in nodules seem to have polygenesis: crystallization from a Fe melt, direct condensation from a fractionated gas, reaction of preexisting phases with a reduced nebular gas, exsolution at subsolidus conditions, and disaggregation of chondrules. Therefore, the origin of opaque-mineral nodules is not simple, and the genesis includes complicated processes which took place in the protosolar nebula.

The concentric structure is a key for resolving the genesis of the concentric nodules, and another key is ubiquitous occurrence of a silica mineral in the middle zone. For the case of a typical concentric nodule of kamacite-core subtype, No. 511 (Fig. 3), the core and mantle consist mainly of kamacite, and the middle zone consists mainly of a silica mineral and kamacite. Hypothesis for the formation of the concentric structure of No. 511 is as follows: the core Fe metal which contained Si more than 2 wt% is a fragment of large Fe metal which was produced by crystallization of a Fe melt or condensed directly from a reduced nebular gas. With decreasing temperatures, a fraction of the Si in the core Fe metal reacted with the nebular gas by reaction (4) to produce a silica mineral in the peripheral portion. After or during formation of a silica mineral, precipitation of Fe-metals from a reduced gas took place to form the mantle Fe metal. The Si contents of kamacite are controlled finally by the exsolution of perryite and schreibersite at a low temperature range.

The middle zone of another concentric nodule No. 502-I (Fig. 1a) includes a silica mineral and niningerite as main phases. A fraction of the silica mineral may be produced by the reaction (4) in the same way as that in No. 511, but the remaining

fraction of the silica mineral might form along with niningerite by the reaction (2).

Some nodules of kamacite-core subtype include a middle zone consisting of forsterite and/or enstatite in addition to a silica mineral (Figs. 2b and 5b). The forsterite and enstatite may have derived from chondrules by disaggregation to attach the core Fe metal.

The other subtype, sulfide-core nodules, seems to have been produced by the following hypothesis; after the formation of niningerite and roedderite by the reactions (2), (3), and (8), they were fragmented and the precipitation of Fe-metal from a reduced gas took place to form the mantle.

The subtypes, Ka, Ka-Tr, Tr, Nin-Tr, and Djer-Tr nodules, show a continuous spectrum on their textures and model compositions. Except for the structure, a remarkable difference between concentric and massive nodules is that the latter type had suffered in various degrees from sulfurization although the former type slightly.

Kamacite in massive nodules (for an example, No. 500) may be fragments of larger metal-troilite aggregates which formed by crystallization from a melt. The troilite is massive and contains high Cr content and daubreelite lamellae. After consolidation and the subsequent fragmentation, they had suffered from sulfurization at low temperatures to produce massive and porous troilites containing low Cr content and being free from daubreelite lamellae, resulting in Ka-Tr or Tr nodules. At lowest temperatures, the reaction (7) took place to produce djerfisherite, and porous troilite which contained the lowest Cr content was produced to include the djerfisherite, resulting in Djer-Tr nodules.

Acknowledgments

I would like to express my thanks to NIPR for the Y-691 sample preparation and the co-operation with the Y-691 consortium studies. I thank Prof. EL GORESY for his kind discussion. This study has been supported by a Grant for Scientific Research, from the Ministry of Education, Science and Culture, Japan.

References

- BARTON, P. B., Jr. and TOULMIN, P., III (1966): Phase relations involving sphalerite in the Fe-Zn-S system. *Econ. Geol.*, **61**, 815-849.
- BENCE, A. E. and ALBEE, A. L. (1967): Empirical correction factors for the electron microanalysis of silicates and oxides. *J. Geol.*, **76**, 382-403.
- BOORMAN, R. S. (1967): Subsolidus studies in the ZnS-FeS-FeS₂ system. *Econ. Geol.*, **62**, 614-631.
- CAMERON, A. G. W. (1973): Abundances of the elements in the solar system. *Space Sci. Rev.*, **15**, 121-146.
- DODD, R. T., VAN SCHMUS, W. R. and MARVIN, U. B. (1965): Merriheite, a new alkali-ferromagnesian silicate from the Mezo-Madaras chondrite. *Science*, **149**, 972-974.
- EL GORESY, A. and KULLERUD, G. (1969): Phase relations in the system Cr-Fe-S. *Meteorite Research*, ed. by P. M. MILLMAN. Dordrecht-Holland, D. Reidel.
- EL GORESY, A. YABUKI, H., EHLERS, K., WOOLUM, D. and PERNICKA, E. (1988): Qinzhen and Yamato 691; A tentative alphabet for the EH chondrites. *Proc. NIPR Symp. Antarct. Meteorites*, **1**, 65-101.
- FEGLY, B., Jr. and LEWIS, J. S. (1980): Volatile element chemistry in the solar nebula; Na, K, F, Cl, Br, and P. *Icarus*, **41**, 439-455.

- FUCHS, L. H. (1966): Djerfisherite, alkali copper-iron sulfide; a new mineral from enstatite chondrites. *Science*, **153**, 166–167.
- FUCHS, L. H., FRONDEL, C. and KLEIN, C., Jr. (1966): Roedderite, a new mineral from the Indarch meteorite. *Am. Mineral.*, **51**, 949–955.
- GROSSMAN, L. and LARIMER, L. W. (1974): Early chemical history of the solar system. *Rev. Geophys. Space Phys.*, **12**, 71–101.
- HONDA, M., BERNATOWICS, T. J. and PODOSEK, F. A. (1983): ^{128}Xe - ^{128}Xe and ^{40}Ar - ^{39}Ar chronology of two Antarctic enstatite meteorites. *Mem. Natl Inst. Polar Res., Spec. Issue*, **30**, 275–291.
- HUTCHISON, M. N. and SCOTT, S. D. (1983): Experimental calibration of the sphalerite cosmobarometer. *Geochim. Cosmochim. Acta*, **47**, 101–108.
- IKEDA, Y. (1988a): Petrochemical study of the Y-691 enstatite chondrite (E3) I; Major element chemical compositions of chondrules and inclusions. *Proc. NIPR Symp. Antarct. Meteorites*, **1**, 3–13.
- IKEDA, Y. (1988b): Petrochemical study of the Y-691 enstatite chondrite (E3) II; Descriptions and mineral compositions of unusual silicate-inclusions. *Proc. NIPR Symp. Antarct. Meteorites*, **1**, 14–37.
- IKEDA, Y. (1989): Petrochemical study of the Y-691 enstatite chondrite (E3) III; Descriptions and mineral compositions of chondrules. *Proc. NIPR Symp. Antarct. Meteorites*, **2**, 75–108.
- KEIL, K. (1968): Chemical and mineralogical relationships among enstatite chondrites. *J. Geophys. Res.*, **73**, 6945–6976.
- KEIL, K. and ANDERSEN, C. A. (1965): Electron microprobe study of the Jajh deh Kot Lalu enstatite chondrite. *Geochim. Cosmochim. Acta*, **29**, 621–632.
- KULLERUD, G. (1958): The Cu-S system. *CIW Year Book*, **57**, 215–218.
- LARIMER, J. W. (1967): Chemical fractionations in meteorites—I; Condensation of the elements. *Geochim. Cosmochim. Acta*, **31**, 1215–1238.
- LARIMER, J. W. and BUSECK, P. R. (1974): Equilibration temperatures in enstatite chondrites. *Geochim. Cosmochim. Acta*, **38**, 471–477.
- LARIMER, J. W. and BARTHOLOMAY, M. (1979): The role of carbon and oxygen in cosmic gases; Some applications of the chemistry and mineralogy of enstatite chondrites. *Geochim. Cosmochim. Acta*, **43**, 1455–1466.
- MULLER, N. and JESSBERGER, E. K. (1985): Laser ^{40}Ar - ^{39}Ar dating of the EH3 Qingzhen chondrite. *Lunar and Planetary Science XVI*. Houston, Lunar Planet. Inst., 595–596.
- OKADA, A. (1975): Petrological studies of the Yamato meteorite. Part 1; Mineralogy of the Yamato meteorites. *Mem. Natl Inst. Polar Res., Spec. Issue*, **5**, 14–66.
- PRINZ, M., NEHRU, M. K., WEISBERG, M. K., DELANEY, J. S. and YANAI, K. (1984): Yamato-691, a Type 3 enstatite chondrite; relationship with other unequilibrated enstatite chondrites (UEC's). *Papers Presented to the Ninth Symposium on Antarctic Meteorites*, 22–24 March 1984. Tokyo, Natl Inst. Polar Res., 14–17.
- RAMBALDI, E. R. and RAJAN, R. S. (1983): Chemical and textural study of Qingzhen, a highly unequilibrated enstatite chondrite. *Lunar and Planetary Science XIV*, Houston, Lunar Planet. Inst., 626–627.
- RAMBALDI, E. R., HOUSLEY, R. M., RAJAN, R. S., CIRLIN, E., EL GORESY, A. and WANG, D. (1983): Unusual mineral assemblages and textures in Qingzhen enstatite chondrite. *Meteoritics*, **18**, 380–381.
- RUBIN, A. E. (1983): The Adhi Kot breccia and implications for the origin of chondrules and silica-rich clasts in enstatite chondrites. *EPSL*, **64**, 201–212.
- RUBIN, A. E. (1984): The Blithfield meteorite and the origin of sulfide-rich, metal-poor clasts and inclusions in brecciated enstatite chondrites. *EPSL*, **67**, 273–283.
- SAXENA, S. K. and ERIKSSON, G. (1983): Low- to medium-temperature phase equilibria in a gas of solar-composition. *EPSL*, **65**, 7–16.
- SEARS, D. W. G. and WEEKS, K. S. (1984): First known EL5 chondrite-*evudebece* for dual genetic sequence for enstatite chondrites. *Nature*, **308**, 257–259.
- SHIMA, M. and SHIMA, M. (1975): Cosmo-chemical studies of the Yamato meteorites; A summary

- of chemical studies on Yamato (A), (B), (C) and (D) meteorites. Mem. Natl Inst. Polar Res., Spec. Issue, **5**, 9–13.
- SKINNER, B. J. and LUCE, F. D. (1971): Solid solutions of the type (Ca, Mg, Mn, Fe)S and their use as geothermometers for the enstatite chondrites. Am. Mineral., **56**, 1269–1296.
- WASSON, J. T. and WAI, C. M. (1970): Composition of the metal, schreibersite and perryite of enstatite chondrites and the origin of enstatite chondrites and achondrites. Geochim. Cosmochim. Acta, **34**, 169–184.
- WEAKS, K. S. and SHEARS, D. W. G. (1985): Chemical and physical studies of type 3 chondrites-V; The enstatite chondrites. Geochim. Cosmochim. Acta, **49**, 1525–1536.

(Received April 15, 1988; Revised manuscript received October 11, 1988)